

## How feasible is climate-resilient building design within the Global South context? Insights from Latin American residential sector

Alexandre Santana Cruz <sup>a</sup>, Rafael Eduardo López-Guerrero <sup>b</sup>, Vítor Freitas Mendes <sup>c,d</sup>, Leopoldo Eurico Gonçalves Bastos <sup>a,e</sup>, Lucas Rosse Caldas <sup>a,\*</sup>

<sup>a</sup> Graduate Program in Architecture (PROARQ), Universidade Federal do Rio de Janeiro (UFRJ), Rio de Janeiro, RJ CEP 21941-972, Brazil

<sup>b</sup> Department of Construction Sciences, Universidad del Bío-Bío, Avda Collao 1202, Concepción, Chile

<sup>c</sup> Graduate Program in Civil Engineering (PROPEC), Universidade Federal de Ouro Preto (UFOP), Ouro Preto, MG CEP 35402-163, Brazil

<sup>d</sup> Instituto Federal de Educação, Ciência e Tecnologia de Minas Gerais (IFMG), Santa Luzia, MG CEP 33115-390, Brazil

<sup>e</sup> Graduate Program in Architecture and City (PPGAC), Universidade Vila Velha, Vila Velha, ES CEP 29102-920, Brazil

### ARTICLE INFO

#### Keywords:

Climate change  
Global South  
Latin America  
Life cycle assessment  
Life cycle cost  
Building performance simulation  
Machine learning  
Optimization

### ABSTRACT

Developing climate-resilient building design is inherently complex, requiring a careful balance between adaptation and mitigation challenges. This study investigates the feasibility of climate-resilient building design in five Latin American cities. Hypothetical future urban weather files are generated by integrating IPCC emissions scenarios with urban heat island (UHI) effects. Extreme Gradient Boosting (XGBoost) and Artificial Neural Networks (ANN) are evaluated as surrogate models, leveraging transfer learning to capture climate-driven thermal-energy performance shifts. The Shapley Additive Explanation (SHAP) method is used to assess how climate change influences the importance of input variables. Then, the surrogate models are coupled with the Non-Dominated Sorting Genetic Algorithm III (NSGA-III) to optimize the building envelope based on the thermal-energy performance, carbon emissions, and total costs. Lastly, the Technique for Order Preference by Similarity to Ideal Solution (TOPSIS) method is used to perform the trade-off analysis, with different weighting factors depending on the preference context. The results showed future urban weather trending towards extreme conditions. XGBoost and ANN yielded promising accurate results, with future urban context significantly influencing the importance of input variables. Despite climate variations, optimal building envelope configurations remained consistent across different cities. Although advanced construction systems offer benefits, their feasibility is limited by cost and carbon emissions. Thus, this study concluded that climate-resilient building design in Latin America is best attained through passive architectural strategies. A good solar orientation, small windows, light-colored envelope, and insulated roof provided a cost-effective, sustainable, and equitable solution to protect vulnerable communities in the Global South.

### 1. Introduction

Over one billion people worldwide lack adequate housing, with the vast majority concentrated in the Global South (GS)—a group of developing nations spanning Latin America, Africa, Asia, and Oceania (excluding Israel, Japan, South Korea, Australia, and New Zealand) [1]. In these regions, population growth, rapid urbanization, and economic inequalities combine with climate change to pose severe risks for vulnerable communities, as highlighted by the IPCC [2–7]. Cooling access is a critical concern: at least one billion people face risks from insufficient cooling, while more than two billion rely on inefficient

devices that drive up energy use and carbon emissions [8–10]. Latin America exemplifies these dynamics—see Fig. 1, which situates the region within the Global North–South paradigm. Despite recent strides in manufacturing, services, and technology—driven by foreign investment and trade agreements [11,12]—the region still faces a housing deficit and the proliferation of informal settlements (slums and favelas) [13]. Local, self-built housing commonly uses affordable materials like clay and limestone in masonry and concrete, which meet urgent shelter needs but often lack resilience against environmental hazards worsened by a warming climate [14–16]. Addressing this intersection of housing shortfall, energy poverty, and climate vulnerability requires

\* Corresponding author.

E-mail address: [lucas.caldas@fau.ufrj.br](mailto:lucas.caldas@fau.ufrj.br) (L. Rosse Caldas).

comprehensive solutions that embed sustainable development, equitable resource access, and climate-resilient, socially inclusive building practices at their core [17–19].

When it comes to buildings, resilience is shaped by four main parameters [20–23]. Vulnerability refers to how easily a building can be damaged by external forces. Adaptability is the ability to adjust to current or future climate conditions and their effects on people. Mitigation focuses on reducing greenhouse gas (GHG) emissions or increasing their absorption and storage. Resistance is a building's capacity to withstand external forces without major damage or loss of functionality [2–7]. Therefore, climate-resilient building design starts with assessing vulnerability, which can guide the creation of adaptation and mitigation strategies to improve resistance to future weather conditions [20–23].

Building performance simulation (BPS) tools are now widely employed to assess resilience, especially for assessing the risk of overheating under changing climate conditions [24]. Instead of using historical datasets, researchers recommend updating weather files to reflect anticipated climate shifts [25,26]. The IPCC Assessment Reports (AR) provide a range of emission scenarios—from the Special Report on Emissions Scenarios (SRES) scenarios in AR3/AR4 [4,5], through the Representative Concentration Pathways (RCP) in AR5 [6], to the Shared Socioeconomic Pathways (SSP) in AR6 [7]—which together model potential future climates. Incorporating these scenarios into weather files for BPS enables detailed exploration of building behavior across diverse future climates, supporting the design of more effective resilience

measures [24–28].

### 1.1. Literature review

Despite significant uncertainty, all IPCC scenarios lean toward a warmer future climate. Hugo [29] used SRES scenarios to evaluate informal settlements in Pretoria, South Africa, predicting up to a 40 % increase in heat stress exposure due to climate change. Xiong et al. [30] applied SSP scenarios to assess residential buildings in China, estimating that cooling energy demand could rise by 20 % by 2060. Verichev et al. [31] analyzed residential buildings in Chile using RCP scenarios, finding that heating energy consumption may decrease by up to 16 %. Likewise, studies utilizing SRES projections in locations like Brazil [32], Mexico [33] and Ghana [34] projected energy demand increases of up to 50 % by 2080.

Moreover, weather files are often derived from remote stations far from urban areas, failing to capture local conditions influenced by UHI effects [31,35]. Alternatives include using data from nearby urban stations or employing tools like the Urban Weather Generator (UWG) to model UHI impacts [36]. For instance, Palme et al. [37] and Litardo et al. [38] reported thermal load increases ranging from 15 % to 200 % in residential buildings across Ecuador, Peru, and Chile due to UHI effects. Liu et al. [39] and Ma and Yu [40] observed energy consumption increases up to 11 % in residential buildings in Singapore and Hong Kong, respectively. Similar results can be found in Maceio, Brazil [41].

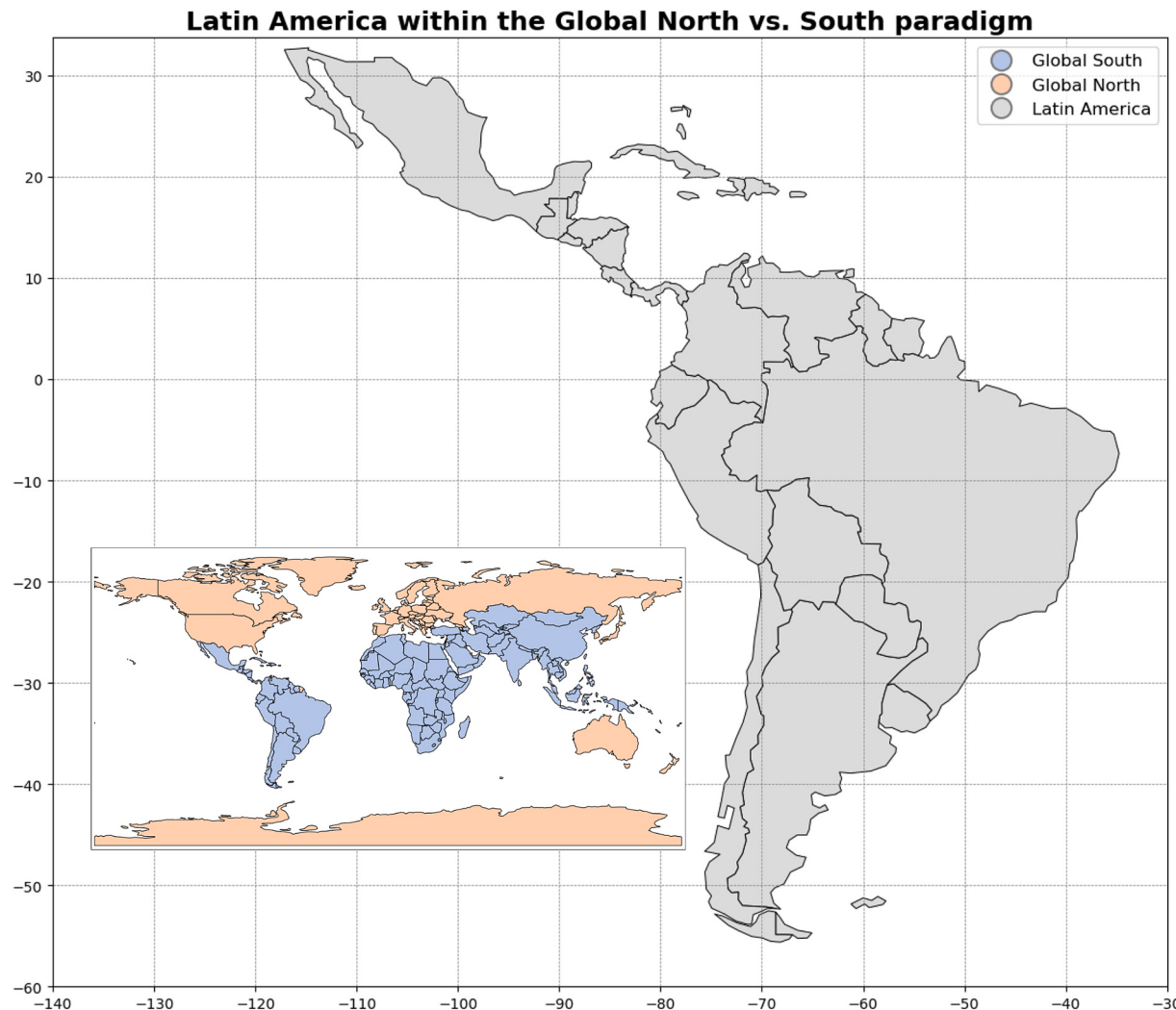


**Fig. 1.** Latin America within the Global North vs. South paradigm.

and Delhi, India [42]. As modern buildings are designed to last at least 50 years [43], it is essential to consider diverse future climate scenarios and the UHI effects to gain valuable insights and guide the development of climate-resilient building designs.

BPS tools are often combined with automation software (e.g., JEPlus + EA, GenOpt, DesignBuilder, and MATLAB) to enhance assessments through parametric analysis, sensitivity analysis, and optimization [44–47]. Although optimization is a powerful technique, it can become computationally expensive when each iteration relies on BPS tools to run energy simulations. A viable alternative is optimization using surrogate models, also referred to as statistical models, meta-models, or response surface approximations [48,49]. These models are trained in pre-existing data to understand the relationships between input and output variables. Once well trained, they replicate the behavior of the original model, enabling quick and accurate predictions for new input scenarios [50–52].

Zou et al. [53] optimized the envelope design of a classroom in Guangzhou, China, using RCP projections. They combined an ANN with the NSGA-II, finding that optimal solutions under future weather conditions tend to lower the SHGC and enhance the thermal insulation of the building envelope. Li et al. [54] optimized a residential building in Huangshan, China, using RCP projections. Different machine learning models such as AdaBoost, Extra Trees, and XGBoost were developed to estimate heating, cooling, and costs, and integrated with NSGA-II for optimization. The optimal solution suggested an increase in roof insulation thickness. Yan et al. [55] used the NSGA-II to optimize the envelope of two residential buildings in Singapore under the SSP projections. The results suggested enhancing thermal insulation to address future warming scenarios. Additionally, the XGBoost algorithm was used with transfer learning techniques to predict the thermal performance of two building types. The transfer learning technique enables a machine learning model to be retrained on new dataset while retaining core insights learned from the initial dataset [56,57]. Essentially, this approach uses the knowledge acquired from one task to improve performance on another related task [58,59].

Optimization often involves addressing multiple conflicting objectives. In this case, a commonly employed approach is the Pareto front that offers decision-makers the flexibility to select the most suitable solution based on their priorities. For instance, Wang et al. [60] investigated retrofit strategies for a residential building in Tianjin, China, selecting the optimal solution based on the shortest payback period. Gonçalves et al. [46] examined construction systems Brazilian social housing located in Belém, evaluating the optimal solutions using cost-benefit ratios. The solution achieved 95 % of the thermal autonomy hours and a notable 31 % reduction in investment costs. On the other hand, several studies apply multi-criteria decision-making (MCDM) techniques to select the preferred solution. For instance, Saryazdi et al. [61] optimized a typical residential building in Kuwait. The TOPSIS-suggested solution achieved reductions in energy consumption, discomfort hours, and carbon emissions of 39 %, 63 %, and 40 %, respectively. Similarly, Song et al. [62] proposed a life cycle retrofit for a rural building in Turpan, China. The TOPSIS-suggested solution enhanced building performance, achieving reductions of 61 %, 53 %, and 14 % in global warming potential, life cycle costs, and discomfort hours, respectively. Chen et al. [63,64] used the Utopia Solution (US) method and the optimization results showed reductions in carbon emissions, discomfort hours, and global cost by up to 50 %, 40 %, and 20 %, respectively.

## 2. Novelty and main contribution

Although Latin America offers fertile ground for collaborative efforts to tackle climate change in the building sector—owing to the housing deficit [14,16], common construction practices [17,18], shared socio-economic conditions [13,15], and regional agreements [11,12] —no studies propose a macro-scale geopolitical analysis. Furthermore,

studies utilizing future urban weather files predominantly focus on adaptation strategies, often neglecting mitigation analysis [19]. Insufficient mitigation efforts increase future adaptation costs, while effective adaptation can reduce mitigation requirements [65]. Synergies emerge when combining multiple measures enhance overall outcomes, though trade-offs may occur if one measure undermines the other [66]. For instance, the higher construction costs for passive designs and the potential for increased carbon emissions from energy-intensive materials [65,66]. In other words, designing climate-resilient buildings is inherently complex, requiring the balancing of multiple, often conflicting objectives to address both adaptation and mitigation challenges. Key considerations include the optimization of thermal performance, energy efficiency, environmental impacts, and costs, where trade-offs must ensure solutions that are sustainable and equitable. Consequently, a pivotal question emerges: How feasible is climate-resilient building design within the GS context?

Therefore, this study investigates the feasibility of climate-resilient building design in five Latin American cities. Hypothetical future urban weather files are generated by integrating IPCC emissions scenarios with UHI effects. XGBoost and ANN are evaluated as surrogate models, leveraging transfer learning to capture climate-driven thermal-energy performance shifts. The SHAP method is used to assess how climate change influences the importance of input variables. Then, these surrogate models are coupled with the NSGA-III to optimize the building envelope based on the thermal-energy performance, carbon emissions, and total costs. Lastly, the TOPSIS method is used to perform the trade-off analysis, with different weighting factors depending on the preference context. As a result, this study delivers two primary innovations: 1) A macro-scale geopolitical perspective designed to stimulate international cooperation, and 2) A simulation-based investigation that integrates machine learning with optimization and MCDM techniques to explore the feasibility of climate-resilient building design in the GS context.

Finally, to provide a clear structure, the remaining sections of this paper are organized as follows: Section 2 outlines the research method conducted, explaining all the steps related to future urban weather predictions, surrogate modeling, optimization and decision-making process. Section 3 illustrates the prediction findings, modeling evaluations, optimization outcomes and decision-making results. Section 4 discusses and compares the results with prior studies. Finally, Section 5 presents the conclusions and directions for future research in the field.

## 3. Method

**Table 1** summarizes the method followed by this study. This summary lists each stage and indicates its objectives, techniques, design variables, and evaluation metrics.

### 3.1. Future urban weather predictions

To capture the rapid urbanization that characterize Latin America's metropolitan areas, this study produced hypothetical future urban weather files for Rio de Janeiro, São Paulo, Santiago, Bogota and Lima, spanning four countries—Brazil, Chile, Colombia, and Peru. These five major urban centers were selected for three reasons: (1) they rank among the largest cities, (2) they exhibit high housing-deficit indices, and (3) they span diverse climate zones. Although these cities do not represent all climate conditions in Latin America, they were selected for their large populations and high projected growth. Baseline climate conditions for each city were drawn from their respective Typical Meteorological Year (TMY) [67], and the key climate parameters, such as dry-bulb temperature (DBT), relative humidity (RH), and global horizontal radiation (GHR), extracted from these files are presented in Table 2 and Fig. 2.

Future climate projections rely on Global Climate Models (GCMs) to simulate interactions within the Earth systems and they are validated

**Table 1**  
Research method.

Index	Stage	Objective	Techniques	Design variables	Evaluation metrics
1	Future urban climate forecast	Forecast future urban weather conditions	• Morphing method. • UHI modeling.	• Location. • SSP emission scenarios. • Urban context. • Weather file. • Envelope properties. • Architectural designs.	• Dry-bulb temperature. • Relative humidity. • Global horizontal radiation. • Thermal load. • SHAP values. • $R^2$ , MAE, and MAPE.
2	Surrogate modeling	Develop machine learning models to predict thermal-energy performance	• XGBoost and ANN. • Transfer learning. • Shapley Additive Explanation.	NSGA-III algorithm.	• Thermal load (TL). • Carbon emissions. • Total cost.
3	Optimization	Optimize thermal-energy performance, carbon, and cost.	NSGA-III algorithm.		
4	Decision-making procedure	Identify the optimal solution for varying preferences	• TOPSIS method • Radar plots	Weighting factors	

**Table 2**  
Historical weather data description [67].

City (Country)	Koppen-Geiger climate classification	DBT (°C)			RH (%)	GHR (Wh/m <sup>2</sup> )
		Max	Min	Mean		
Rio de Janeiro (Brazil)	Aw	38	13	24	82	209
Sao Paulo (Brazil)	Cfa	33	7.5	19	82	213
Santiago (Chile)	Csb	33	-6	15	71	204
Bogota (Colombia)	Cfb	24	0	13	80	184
Lima (Peru)	BWh	30	11	19	81	178

against historical data before using IPCC emissions scenarios [68,69]. Yet, due to their coarse resolution and biases, GCM outputs require a downscaling approach for BPS tools [28]. The downscaling methods can be statistical (stochastic or imposed offset techniques) or dynamical [26]. While stochastic and dynamical methods are computationally intensive [68,70], the statistical imposed offset technique (morphing method) offers an efficient alternative [25,27,68]. Therefore, to address uncertainties in future projections, this study considered the Future Weather Generator tool that applies the morphing method to generate future weather files [28]. The tool is based on CMIP6 and presents Shared Socioeconomic Pathways (SSP) scenarios for 2050 and 2080.

Furthermore, this study utilized the open-access UWG tool, which blends local microclimate data, urban morphology, vegetation, and building characteristics to incorporate UHI effects into weather files [71–73]. These inputs were tailored to reflect the typical low- and medium-rise residential urban layouts in Latin American cities. Two main criteria guided the definition of the urban parameters. First, the urban configuration is classified using the Local Climate Zone (LCZ) system [74]. The compact mid-rise class (LCZ2) was combined with the open mid-rise class (LCZ5) to define LCZ2<sub>5</sub>, representing low-rise apartment context. Similarly, the compact low-rise class (LCZ3) was combined with the open low-rise class (LCZ6) to define LCZ3<sub>6</sub>,

representing detached house context. This classification considered that Latin American cities are characterized by heterogeneous urban fabrics [37,38,75]; and the LCZ subcategories with favorable urban conditions helps mitigate the overestimation of UHI effects [73,75]. Following previous studies [41,76–78], the primary urban parameters were standardized across all cities to ensure consistency and comparability. These parameters included green coverage (GC) of 0.25, average building height (ABH) of 12 m and 5 m, site coverage ratio (SCR) of 0.5, façade-to-site ratio (FSR) of 0.85 and 0.75, and anthropogenic heat from traffic (AHT) of 25 W/m<sup>2</sup> for LCZ2<sub>5</sub> and LCZ3<sub>6</sub>, respectively. Finally, by combining future climate projections with UHI effect, hypothetical future urban weather files were generated to assess how climate change may influence climate-resilient building design.

### 3.2. Surrogate modeling

This study developed surrogate models to predict the TL of two architectural designs under different weather conditions. The process to develop a surrogate model using simulation data involves few steps [48,49]. First, the building-design problem must define the input and output variables. Second, a high-fidelity baseline model needs to be simulated using a sampling technique that effectively captures the design space to build a dataset. The resulting dataset is then pre-processed and divided with k-fold cross-validation for robustness [50]. Third, an appropriate machine learning algorithm is selected, trained on the training set and its performance is validated on the test set using standard metrics [51]. Yet, if its performance is inadequate, the refinement process might involve hyperparameter tuning or additional data [52]. Lastly, once it is validated, the model supports fast optimization and real-time prediction, drastically cutting computational cost.

#### 3.2.1. Architectural designs

Although detached houses still dominate the residential stock, the growing mix of low-, mid-, and high-rise developments in urban areas makes it essential to study diverse architectural typologies to verify the broad relevance of our findings [54,79–83]. Therefore, this study evaluated two representative architectural designs: a detached house (DH)

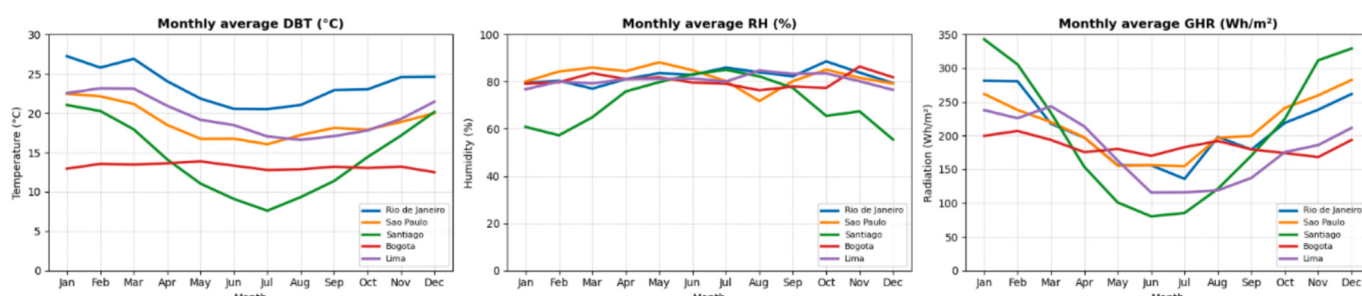


**Fig. 2.** Monthly average values of historical weather data [67].

and a low-rise apartment (LRA) [75,84]. Fig. 3 presents 3D renderings and floor plans of the two models, each with a 3 m ceiling height and floor areas of 56 m<sup>2</sup> and 62 m<sup>2</sup>, respectively.

The DH model was calibrated with data from prior studies [75,84], and the LRA adopted the same configuration parameters to achieve comparable accuracy. Without calibration, accuracy is sustained by validated software, precise inputs, and baseline checks that expose input or modeling errors [85]. Therefore, all models were developed using EnergyPlus, a validated simulation tool, with key inputs aligned to building regulation standards and calibrated results [86]. For example, the thermal zones accounted for occupancy of two to four people with a metabolic rate of 108 W/person, a lighting power density of 6 W/m<sup>2</sup>, and a constant equipment load of 1.5 W/m<sup>2</sup> [86].

Because the DH sits directly on the soil, variations in ground temperature strongly shape their thermal behavior. In contrast, this heat exchange is less relevant in apartments, as the residential unit may not be in direct contact with the ground. Accordingly, the DH model considered soil temperature generated using the EnergyPlus Slab Program, whereas the LRA used an adiabatic ground boundary. As shown in Fig. 3, we modeled only the top floor for simplicity. Furthermore, occupant behavior is a critical factor that can cause inaccuracies in thermal-energy performance assessments. In this study, the occupancy schedule was defined as occupants always being home, illustrating a work-from-home scenario. This approach was chosen to represent a worst-case scenario for occupancy-generated heat, with a higher tendency for overheating risks [85,87]. Section 2.3.1 explains how EnergyPlus was used to calculate the TL metric, which represents the amount of heat that must be added or removed to maintain thermal comfort conditions.

### 3.2.2. Design variables

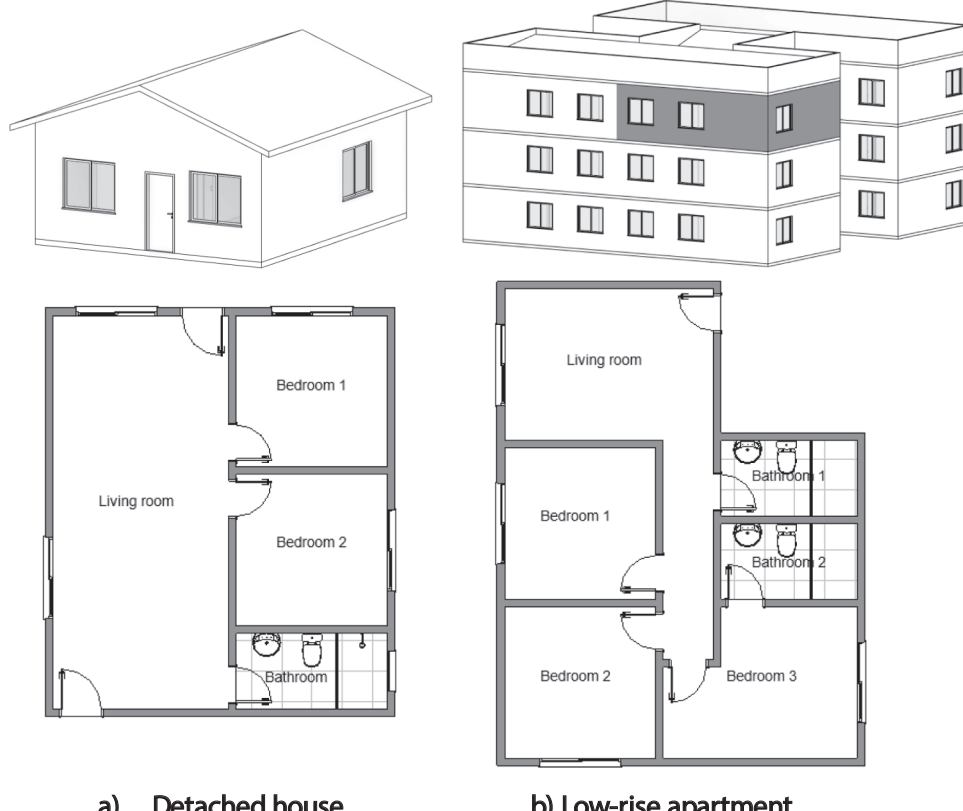
While the study incorporated the most common construction systems used in the residential sector, it also explored emerging technologies

available in the market. Table 3 describes the thermal properties for all wall, roof, ceiling and glazing types considered in this study. Specifically, Insulated Concrete Forms (ICF), Structural Concrete Insulated Panels (SCIP), Steel Frame, and Wood Frame systems were considered as potential options for walls. ICF and SCIP walls feature expanded polystyrene (EPS) blocks/panels that serve as permanent formwork for reinforced concrete. Both durable construction configurations provide excellent thermal and sound insulation, enhanced energy efficiency, and simplified construction processes [88,89]. Steel and wood frame systems consist of steel or wooden studs and beams, typically insulated and sheathed with materials such as rock wool, oriented strand board (OSB), or cement/plaster board. These systems offer advantages such as improved thermal performance and ease of construction [90]. Wood framing is renewable and provides good insulation, while steel framing is more resistant to moisture and pests [91]. Finally, the complete list of design variables, along with their respective value ranges, is further detailed in Table 4.

### 3.2.3. Dataset

The dataset creation step selects design points to maximize information gain while minimizing sampling time. While Latin Hypercube Sampling (LHS) is popular [48,49], Sobol's method is superior for generating low-discrepancy quasi-random sequences, offering uniform input space coverage. This advantage reduces clustering, achieves faster convergence with fewer samples, and ensures scalability and reproducibility, making Sobol ideal for complex, high-dimensional models [63,64].

This study examined two distinct building types within two climate contexts: historical and future urban weather. Consequently, four datasets were required for each evaluated city. The combinations of all design variables listed in Table 4 resulted in 10<sup>6</sup> possible scenarios per dataset. However, generating such extensive datasets is resource-intensive and time-consuming. To optimize the balance between



a) Detached house

b) Low-rise apartment

Fig. 3. 3D renderings and floor plans for: (a) Detached house, and (b) Low-rise apartment.

**Table 3**

Thermal properties of the construction systems.

Component	Index	Construction system	Description (Layers)	Thickness (m)	Specific gravity (kg/m³)	Thermal conductivity (W/mK)	Specific heat (kJ/kgK)
Wall	W1	Traditional masonry	Coating mortar	0.02	1950	1.15	1.00
			Ceramic blocks (horizontally perforated)	0.09	459	0.47	0.93
			Coating mortar	0.02	1950	1.15	1.00
		Concrete block	Construction system's properties: U-value = 2.77 W/(m²K) and TC = 117 kJ/(m²K)				
			Coating mortar	0.02	1950	1.15	1.00
			Concrete blocks (vertically perforated)	0.14	840	1.01	1.00
	W3	Concrete wall	Coating mortar	0.02	1950	1.15	1.00
			Construction system's properties: U-value = 2.73 W/(m²K) and TC = 195 kJ/(m²K)				
	W4	Insulated Concrete Forms	Cast-in-place concrete wall	0.10	2300	1.75	1.00
			Construction system's properties: U-value = 4.40 W/(m²K) and TC = 230 kJ/(m²K)				
			Coating mortar	0.02	1950	1.15	1.00
			EPS board	0.05	2300	1.75	1.00
			Concrete	0.10	2300	1.75	1.00
W5	Structural Concrete Insulated Panels	W5	EPS board	0.05	2300	1.75	1.00
			Coating mortar	0.02	1950	1.15	1.00
			Concrete	0.05	2300	1.75	1.00
			EPS board	0.05	2300	1.75	1.00
			Concrete	0.05	2300	1.75	1.00
	W6/ 7	Wood/Steel frame	Coating mortar	0.02	1950	1.15	1.00
			Construction system's properties: U-value = 0.40 W/(m²K) and TC = 325 kJ/(m²K)				
			Cement board	0.01	2300	1.75	1.00
			OSB	0.02	1500	1.15	1.00
			Rock wool	0.05	20	0.045	0.75
Roof	R1	Fiber cement tiles	Air gap	—	—	—	—
	R2	Clay tile	OSB	0.02	1500	1.15	1.00
	R3	Thermoacoustic metal tile	Cement board	0.01	2300	1.75	1.00
			Construction system's properties: U-value = 0.6 W/(m²K) and TC = 116 kJ/(m²K)				
			Metal tiles	0.006	1700	0.65	0.84
Ceiling	R4	Metal tiles	Metal tiles	0.01	1500	1.15	1.00
	C1	Plaster panel	EPS board	0.01	7800	55	0.46
	C2	Wooden lining	Metal tiles	0.01	7800	55	0.46
	C3	Polyvinyl chloride (PVC) board					
	C4	Concrete					
Glazing	C5	EPS board					
	C1	Simple glazing					
	C2	Double pane glazing (low-e)					
	C3	Triple pane glazing (low-e)					

**Table 4**

Overview of design variables.

Category	ID	Description	Unit	Range
Envelope	DV1	Orientation	(°)	{0, 45, 90, 135, 180, 225, 270, 315}
	DV2	Wall type	Dimensionless	{1, 2, 3, 4, 5, 6, 7} – See Table 3
	DV3	Roof type	Dimensionless	{1, 2, 3, 4} – See Table 3
	DV4	Ceiling type	Dimensionless	{1, 2, 3, 4, 5} – See Table 3
	DV5	Glazing type	Dimensionless	{1, 2, 3} – See Table 3
	DV6	WWR	%	{20, 30, 40, 50, 60}
	DV7	Absorptance value – Wall	Dimensionless	{0.2, 0.3, 0.4, 0.5, 0.6, 0.7, 0.80}
	DV8	Absorptance value – Roof	Dimensionless	{0.2, 0.3, 0.4, 0.5, 0.6, 0.7, 0.80}

simulation time and data requirements for transfer learning, different sample sizes were used for each weather context [55]. More specifically, for each city two sample sizes were generated, the first one with a total of 1000 samples for the historical weather context and the second with a total of 500 for the future urban weather context. This approach

hypothesized that the historical dataset would capture the relationship between input variables and output, and the smaller future urban dataset would effectively reflect the shifts in TL driven by climate change.

To validate this hypothesis, the SHAP method evaluated the contribution of each input variables when considering different weather contexts. Based on cooperative game theory, the SHAP method quantifies the input variable's contribution to model predictions, offering global and local interpretability, and making it a robust and versatile tool [92]. This study used it as a sensitivity analysis to examine how climate change may influence the importance of input variables, providing insights into potential shifts in the thermal-energy performance metric.

Each dataset then underwent preprocessing to ensure that features with larger numerical ranges did not overly affect the model's predictions. To give every feature equal weight, standard z-score scaling was applied (Equation 1), where  $\mu$  represents the sample mean and  $\sigma$  the associated standard deviation.

$$z = \frac{x - \mu}{\sigma} \quad (1)$$

### 3.2.4. Transfer learning

The transfer learning process involves two primary steps: first, training the model on the source domain, and second, refining it for the target domain [56,57]. This study adopted the historical dataset as source domain and the future urban dataset as target domain. In a technical explanation, the procedure begins with source and target tasks ( $T_s$  and  $T_t$ ), each associated with their respective datasets ( $D_s$  and  $D_t$ ). In supervised learning, a given task T has two elements: a labeled space (Y) and a predictive function  $f(x)$  that maps an input (x) to an output (y). The model trained on the source task  $f_s(x)$  extracts features  $h(x)$  from the source data, which are then adapted to build a new target-specific model  $f_t(x)$ . This target model integrates the feature extractor with a new task-specific component ( $g(\cdot)$ ) as shown in Equation 2). In this context, the fine-tuning step involves adjusting the pre-trained model's parameters  $\theta_s$  to suit the target task by minimizing a loss function ( $L$ , as defined in Equation 3). However, during the fine-tuning step, only a subset of parameters ( $\theta_t$ ) is updated, preserving the general knowledge captured in  $\theta_s$ . Therefore, the goal is to reduce the loss on the target dataset ( $D_t$ ) using the sample-wise loss function  $l(\cdot)$  [58,59].

$$f_t(x) = g(h(x)) \quad (2)$$

$$L(f_t(x_t), y_t) = \frac{1}{N_t} \sum_{j=1}^{N_t} l(f_t(x_t^j), y_t^j) \quad (3)$$

This study focused on two machine learning algorithms: XGBoost and ANN. The XGBoost, a powerful gradient boosting algorithm, constructs decision trees sequentially, with each tree correcting the produced errors of the previous ones. By optimizing a custom loss function and incorporating regularization, it achieves high accuracy while mitigating overfitting [93]. Although the XGBoost applies ensemble learning to bridge errors between domains, transfer learning is often associated with deep learning models. Therefore, ANN is also considered in this study. An ANN consist of an input layer, with one or more hidden layers, and an output layer, with interconnected neurons that process data through activation functions [94]. By freezing the early layers to preserve learned general features and fine-tuning the later layers, the ANN efficiently adapts to new tasks while maintaining foundational knowledge [57].

Effective hyperparameter optimization is essential for achieving robust surrogate models [48]. This study opted for random search because it is easy to implement, scales well in high-dimensional spaces, and delivers better results than grid search without the added complexity of Bayesian or evolutionary methods. For XGBoost, we tuned the number of trees, maximum tree depth, and learning rate [93]; for the ANN, we adjusted the number of hidden layers, neurons per layer, activation functions, and learning rate [94]. The implementation utilized Python libraries such as TensorFlow, Scikit-learn, and XGBoost.

### 3.2.5. Performance evaluation

Machine learning models are evaluated based on their ability to replicate the learned behavior on unseen data [48,49]. Therefore, this study adopted three performance evaluation metrics: (1) the coefficient of determination ( $R^2$ ) that reflects the share of variance the model explains, with values close to 1 signifying a strong fit; (2) the mean absolute error (MAE) that conveys the average magnitude of the residuals in the response output variable's units; and finally, (3) the mean absolute percentage error (MAPE) that normalizes those MAE errors as percentages, enabling comparisons across datasets of different scales. These metrics are derived from Equation 4 to 6, where  $y_i''$  is the predicted value,  $y_i'$  is the observed value;  $y_i$  is the arithmetic mean of y; and n the number of test samples.

$$R^2 = 1 - \frac{\sum_i^n (y_i - y_i'')^2}{\sum_i^n (y_i - y_i'')^2} \quad (4)$$

$$MAE = \frac{1}{n} \sum_i^n |y_i - y_i'| \quad (5)$$

$$MAPE = \frac{1}{n} \sum_i^n \left| \frac{y_i - y_i'}{y_i} \right| \quad (6)$$

In addition, the models' performance was evaluated with cross-validation rather than a single train-test split. The data were partitioned into k folds so that every observation served alternately for training and validation. Averaging the metrics across all folds yields a more dependable estimate of generalizability and helps curb both over- and under-fitting [50,51].

### 3.3. Optimization

The goal of this study was to evaluate the feasibility of climate-resilient design within the GS context, with a particular focus on Latin America. To achieve this, different building envelope systems (See Table 3) were examined to understand their impact on thermal-energy performance, carbon emissions, and costs. This study considered the NSGA-III to address the lack of adoption of emerging algorithms in the BPS research field [95,96]. The NSGA-III is designed to handle problems with more than two objectives, by extending the NSGA-II when introducing reference points to guide the search process and ensure diversity in the solution set [97]. The algorithm begins with an initial population, evaluates fitness based on Pareto dominance, and applies selection, crossover, and mutation to evolve solutions. Its key advantage lies in the ability to maintain a well-distributed set of solutions along the Pareto front, making it suitable for high-dimensional problems. Additionally, its reference-point-based approach improves scalability and convergence compared to earlier algorithms. Finally, the Python library Pymoo was used to implement NSGA-III with Das-Dennis reference directions, mixed-variable sampling and mating, duplicate elimination, and 300 generations.

#### 3.3.1. Thermal performance

Natural ventilation has predominated in Latin America [11–14,16]; yet recent economic growth is spurring wider adoption of HVAC systems [8–10]. Coordinating HVAC systems with natural airflow is complex: although enhanced envelope insulation boosts energy efficiency, it can also exacerbate overheating unless passive measures are incorporated [98–100]. Therefore, this study combined the Airflow Network object with the Ideal Loads Air System object in EnergyPlus to calculate the TL metric [100]. The Airflow Network object simulates infiltration driven by wind-induced pressure differences, even when windows and doors are closed (through cracks), as homes in Latin America are typically not well sealed. Meanwhile, the Ideal Loads Air System object represents an ideal HVAC system, without incorporating efficiency coefficients, and operates only during occupied hours according to a thermostat schedule. This approach enables more accurate load estimation, supporting the optimization of thermal performance and energy efficiency in building designs [101].

The performance metric used was the TL for combined cooling and heating, as defined in Equation 7.  $TL_{total}$  represents the amount of heat, expressed in  $\text{kWh/m}^2$ , that must be added ( $TL_{heating}$ ) to or removed ( $TL_{cooling}$ ) from all zones per square meter ( $A_{total}$  that refers to the total floor area of the building) to maintain thermal comfort based on a set-point of 20 °C for heating and 25 °C for cooling. Consequently, lower  $TL_{total}$  values indicate better thermal performance and are the desired outcome.

$$TL_{total} = \frac{\sum TL_{cooling} + \sum TL_{heating}}{A_{total}} \quad (7)$$

### 3.3.2. Carbon performance

Carbon emissions for the envelope design were estimated using the Life Cycle Assessment (LCA) methodology. According to ISO 14040:2006, a systematic LCA involves four main steps: (1) defining goals and scope, (2) analyzing the Life Cycle Inventory (LCI), (3) conducting the Life Cycle Impact Assessment (LCIA), and (4) interpreting the results [102]. The goal of the carbon assessment in this study was to quantify kgCO<sub>2</sub>-eq associated with the production and construction of the envelope setup for each architectural model. The scope of assessment focused on the production phase of the life cycle, covering climate change impacts from raw material extraction to fabrication, as well as the transportation of materials to the construction site (A1–A4), according to EN 15804:2019 [103].

For the LCI, this study utilized the Ecoinvent database v.3.8 since different countries are evaluated. Ecoinvent has a broader range of material data and ensures consistency and comparability across all study locations [104]. The total carbon emissions for each element and the overall construction solution were calculated using Equations 8 and 9. In these equations,  $CE_w$ ,  $CE_r$ ,  $CE_c$  and  $CE_g$  represent the carbon emissions for walls, roofs, ceilings, and glazing, respectively.  $CE_i$  denotes the carbon emissions of the  $i^{th}$  component of an element,  $AV_i$  is the built area or volume of the element,  $n$  is the number of components considered for each element, and  $CE$  is the total carbon emission for the considered elements. In the LCIA, EN 15804:2019 method is used. The results, expressed in kilograms of CO<sub>2</sub> equivalent (kgCO<sub>2</sub>-eq), account for GHG such as CO<sub>2</sub>, Nitrogen dioxide (NO<sub>2</sub>), Methane (CH<sub>4</sub>) and other GHGs. Fig. 4 presents the total carbon emissions for each building element in the two architectural designs considered in this study. The takeoff of these elements was derived from a Building Information Modeling (BIM) model using Autodesk Revit. Appendix A provides the surface areas of each envelope system for both architectural models and lists the materials comprising the construction systems explored in this study, along with their respective carbon emission values and units.

$$CE_{w,r,c,g} = \sum_{i=1}^n CE_i \times AV_i \quad (8)$$

$$CE = CE_w + CE_r + CE_c + CE_g \quad (9)$$

### 3.3.3. Cost performance

To calculate the associated costs for each architectural model, an inventory of all materials used in the envelope systems was created using various databases that provide estimated prices for construction inputs. The National Survey/Database System for Construction Costs and Indices were utilized [105–108]. The costs of elements not found in these databases were obtained through local market quotations and labor costs were excluded from the analysis. Variations in purchase values were observed depending on the building's location; therefore, Fig. 5 illustrates the range of purchase values for each envelope system considered in this study, identified by their IDs (see Table 3). The official currencies of Brazil, Chile, Colombia, and Peru are the Brazilian Real (BRL), Chilean Peso (CLP), Colombian Peso (COP), and Peruvian Sol (PEN), respectively. For the cost analysis, all costs were converted to BRL to ensure consistency and facilitate a comprehensive evaluation.

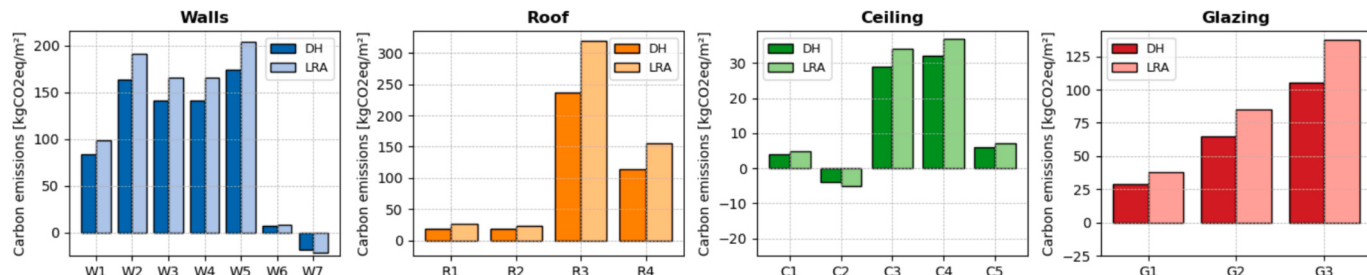


Fig. 4. Carbon emissions for each envelope system.

The total cost for each element and the overall construction cost were calculated using Equations 10 and 11. In these equations,  $TC_w$ ,  $TC_r$ ,  $TC_c$  and  $TC_g$  represent the costs for walls, roofs, ceilings, and glazing, respectively;  $C_i$  is the cost of the  $i^{th}$  component of an element,  $A_i$  is the built area of the element,  $n$  is the number of components considered for each element, and  $TC$  is the total construction cost for the considered elements.

$$TC_{w,r,c,g} = \sum_{i=1}^n C_i \times A_i \quad (10)$$

$$TC = TC_w + TC_r + TC_c + TC_g \quad (11)$$

### 3.4. Decision-making process

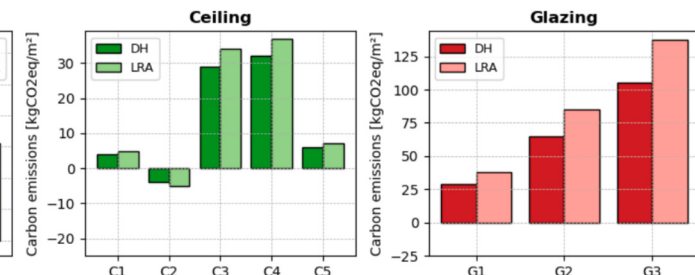
In this study, the final step emphasized the decision-making process to identify the optimal solution within the Pareto front for various preference contexts. A decision-making approach is often required to identify the optimal solution [109,110]. Common approaches include subjective or constrained selection, and weighted sum [48]. However, the MCDM is preferred for its structured, objective, and adaptable approach to balance multiple criteria [61,62]. Therefore, the TOPSIS method was selected due to its flexibility in weighting criteria, robustness in complex scenarios, and clear, interpretable rankings make it widely applicable and practical. TOPSIS evaluates alternatives based on their proximity to the ideal solution and distance from the worst solution, considering both positive and negative values [111]. In addition, it is important to normalize results, as varying ranges among objectives can disproportionately influence the final selection [63,64]. Finally, the trade-off analysis applied different weighting factors for each metric to evaluate how different preferences shape the definition of an optimal solution within a given context. Table 5 outlines the preference contexts considered in this study, along with their descriptions. To enhance result visualization and interpretation, radar plots are utilized at this stage.

## 4. Results

### 4.1. Future urban weather predictions results

In the first step, the study explored the future projections. Although the Future Weather Generator tool provides projections for 2050 and 2080, this study focuses exclusively on 2080. The selected scenarios—SSP1-2.6, SSP2-4.5, SSP3-7.0, and SSP5-8.5—were used to assess the impact of future climate conditions. Fig. 6 presents the monthly average values of DBT, RH, and GHR for each city, providing a comparative overview of the projected climate conditions for all SSP scenarios across all evaluated cities.

Fig. 6 illustrates an increase in the climate parameters analyzed when comparing historical data and future projections. The following results are presented as ranges as they depend on the SSP scenario considered. The DBT is projected to increase between 1.3 °C to 2.71 °C in Rio de Janeiro, 1.3 °C to 2.85 °C in São Paulo, 1.7 °C to 3.63 °C in Santiago, 1.7°C to 3.4 °C in Bogota, and 1.9 °C to 3.36 °C in Lima. The RH is expected to rise between 0.30 % to 1.39 % in Rio de Janeiro, 0.15



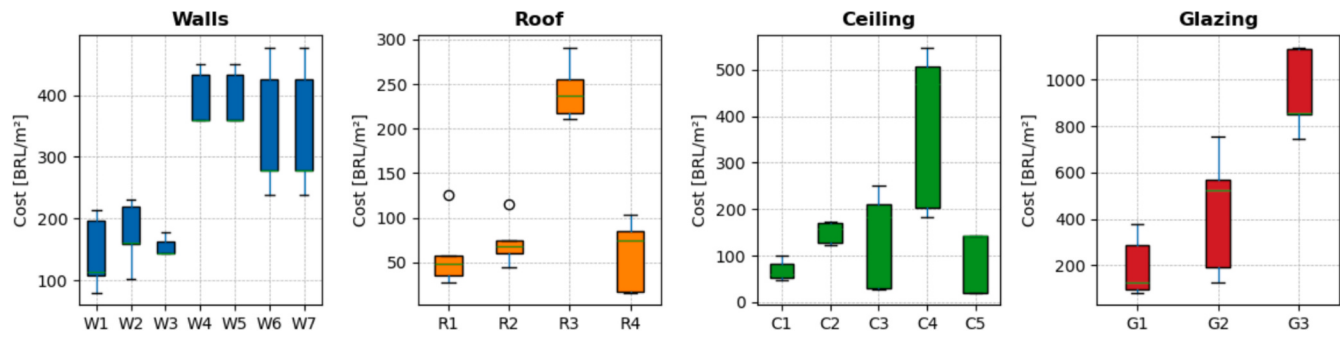


Fig. 5. Range of purchase value for each envelope construction system.

Table 5

Preference contexts considered in this study, along with their criteria descriptions.

Index	Preference context	Criteria description	Weighting factors
1	Thermal load	The best solution in terms of TL metric.	[TL = 1, CE = 0, TC = 0]
3	Carbon emissions	The best solution in terms of CE metric.	[TL = 0, CE = 1, TC = 0]
4	Total Cost	The best solution in terms of TC metric.	[TL = 0, CE = 0, TC = 1]
5	Equal weights	The best solution in terms of TL, CE, and TC metrics	[TL = 1/3, CE = 1/3, TC = 1/3]

% to 1.2 % in Sao Paulo, 4.9 % to 9.2 % in Santiago, 0.8 % to 2.4 % in Bogota, and 0.6 % to 1.4 % in Lima. Similarly, the GHR is projected to increase between 0.9 Wh/m<sup>2</sup> to 2.3 Wh/m<sup>2</sup> in Rio de Janeiro, 0.6 Wh/m<sup>2</sup> to 2.0 Wh/m<sup>2</sup> in Sao Paulo, 2.3 Wh/m<sup>2</sup> to 5.3 Wh/m<sup>2</sup> in Santiago, 0.3 Wh/m<sup>2</sup> to 2.5 Wh/m<sup>2</sup> in Bogota, and 0.4 Wh/m<sup>2</sup> to 2.2 Wh/m<sup>2</sup> in Lima. Finally, for the next step, this study considered only the SSP5-8.5 scenario as it represents the most severe weather conditions.

Moreover, the UWG tool was used to incorporate UHI effects, representing the urban contexts of a LRA (LCZ<sub>25</sub>) and DH (LCZ<sub>36</sub>). Fig. 7 presents the distribution of DBT and Table 6 summarizes the average DBT for the historical, future, and future + urban LCZ<sub>25</sub>, and future + urban LCZ<sub>36</sub> contexts for all analyzed cities.

As data is often sourced from rural areas or distant stations, Table 6 shows that historical weather files exhibited the lowest average DBT values compared to those combined with future projections and UHI models. In addition, when comparing different UHI models, the LCZ<sub>25</sub>

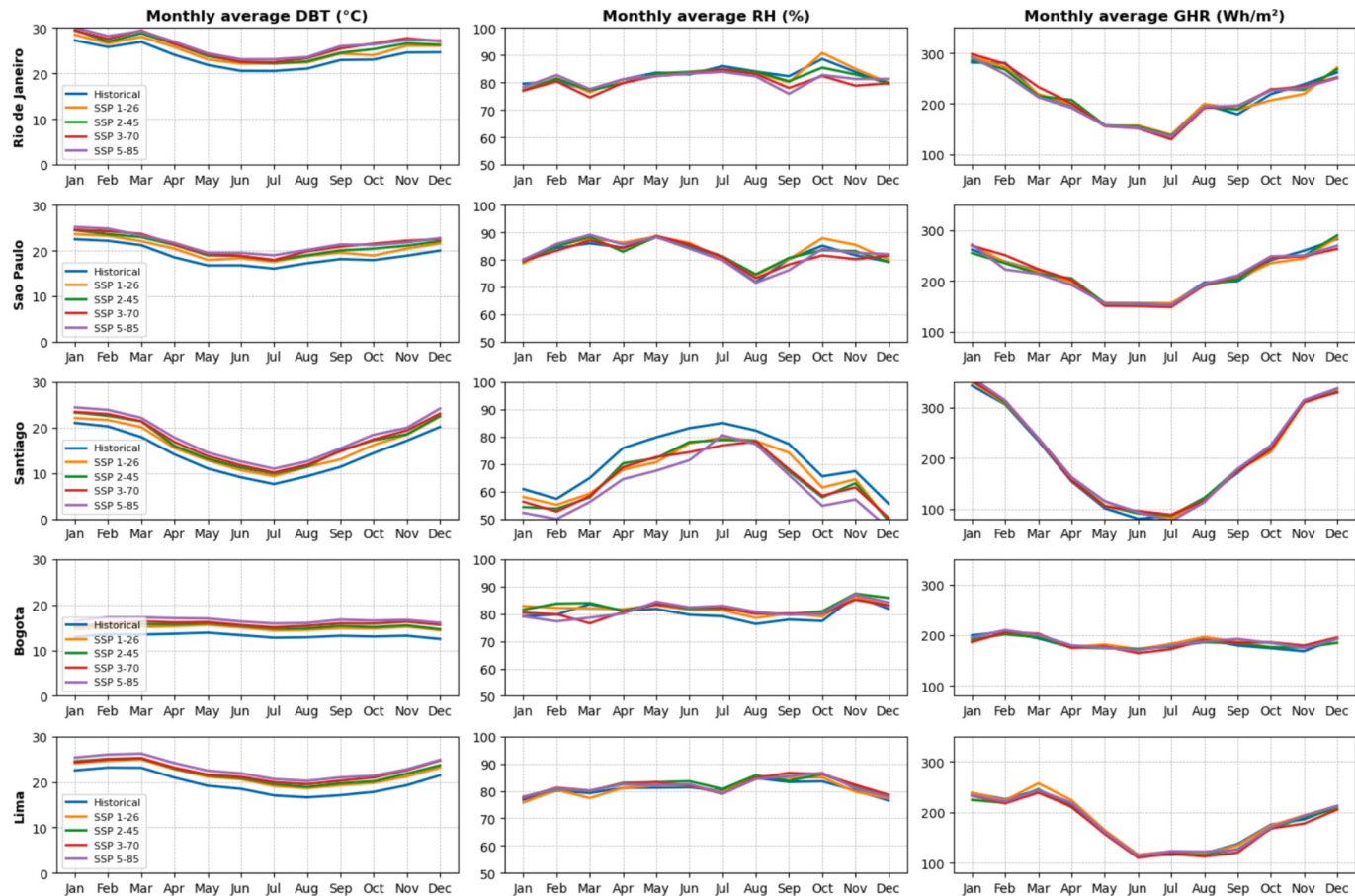
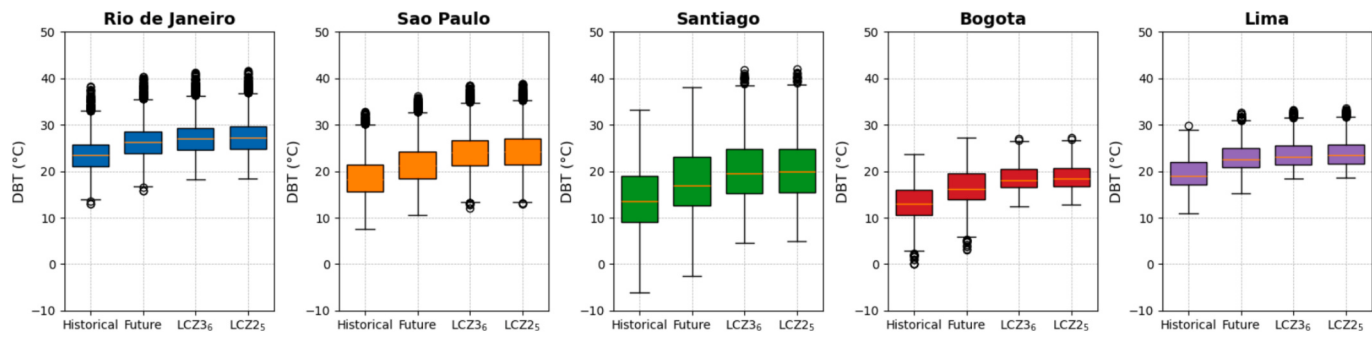


Fig. 6. Monthly average values for DBT, RH, and GHR for 2080 under different SSP projections.



**Fig. 7.** Distribution of DBT values for historical, future, future urban LCZ2<sub>5</sub>, and future urban LCZ3<sub>6</sub> weather contexts.

**Table 6**

Average values of DBT for 2080 under historical, future, and future + urban weather contexts.

City	Average DBT Historical	Future (SSP5-8.5)	Future + Urban (LCZ2 <sub>5</sub> )	Future + Urban (LCZ3 <sub>6</sub> )
Rio de Janeiro	23.6 °C	26.3 °C	27.1 °C	27.4 °C
Sao Paulo	18.9 °C	21.6 °C	24.1 °C	24.4 °C
Santiago	14.4 °C	18.0 °C	20.4 °C	20.6 °C
Bogota	13.2 °C	16.6 °C	18.5 °C	18.8 °C
Lima	19.7 °C	23.0 °C	23.7 °C	23.9 °C

and LCZ3<sub>6</sub> produced highly comparable results. Consequently, for the cities of Rio de Janeiro, Sao Paulo, Santiago, Bogota, and Lima, future urban projections suggest increases in average DBT up to 3.8 °C, 5.5 °C, 6.2 °C, 5.6 °C, and 4.2 °C, respectively. The average DBT difference between historical and future climates is up to 3 °C across all cities. However, this difference rose up to 6 °C with the inclusion of the UHI effect. These findings underscore the importance of creating climate models that can inform the development of climate-resilient building design.

#### 4.2. Surrogate modeling results

In this study, machine learning models were developed to predict the TL of two architectural designs under different weather contexts. The following sections present the results, detailing dataset analysis, the performance evaluation of the machine learning models, and the sensitivity analysis results.

#### 4.3. Data analysis

**Fig. 8** presents the dataset generated that refers to the TL results from each city analyzed. The graphs display the distribution of the TL metric

for the DH and LRA under different weather contexts, respectively.

The variations seen in **Fig. 8** reflect the different climate contexts examined in this study. In addition, the distinct performance between the DH and the LRA is attributed to ground contact, which affects heat exchange within the built environment. Under historical context, Santiago and Bogota exhibited the poorest performance, while Rio de Janeiro, Sao Paulo, and Lima achieved the best results for both architectural designs. In future urban context, Sao Paulo and Lima continued to demonstrate the best performance, whereas Rio de Janeiro experienced the most significant decline. Meanwhile, Santiago and Bogota showed improved results. These findings indicated that as temperatures rise in colder climates like Santiago, heating energy demand decreased, leading to more comfortable indoor temperatures, and consequently, lower TL metric values. Conversely, in warmer climates, the TL metric increased due to the rising demand for cooling. For Rio de Janeiro, the mean deviation of the TL metric between the historical and future urban weather contexts was 150 % for the DH and 123 % for the LRA, with deviations between architectural models reaching up to 54 %. In Sao Paulo, these deviations were 34 % for the DH and 67 % for the LRA, while differences between architectural models reach 80 %. For Santiago, the respective deviations were -57 % and -50 %, with architectural model variations up to 21 %. In Bogota, deviations were -83 % for the DH and -75 % for the LRA, with architectural model differences reaching 46 %. Finally, for Lima, the TL metric deviation was 30 % for the DH and 63 % for the LRA, while architectural model variations peaked at 117 %.

#### 4.3.1. Performance evaluation results

**Table 7** presents the performance evaluation of each machine learning model developed across all cities, with the historical context used as the source domain and future urban context used as target domain, respectively.

**Table 7** highlights the similar performance of XGBoost and ANN in surrogate modeling. Particularly, XGBoost achieved slightly better results for R<sup>2</sup>, MAE, and MAPE metrics across TL model in all cities.

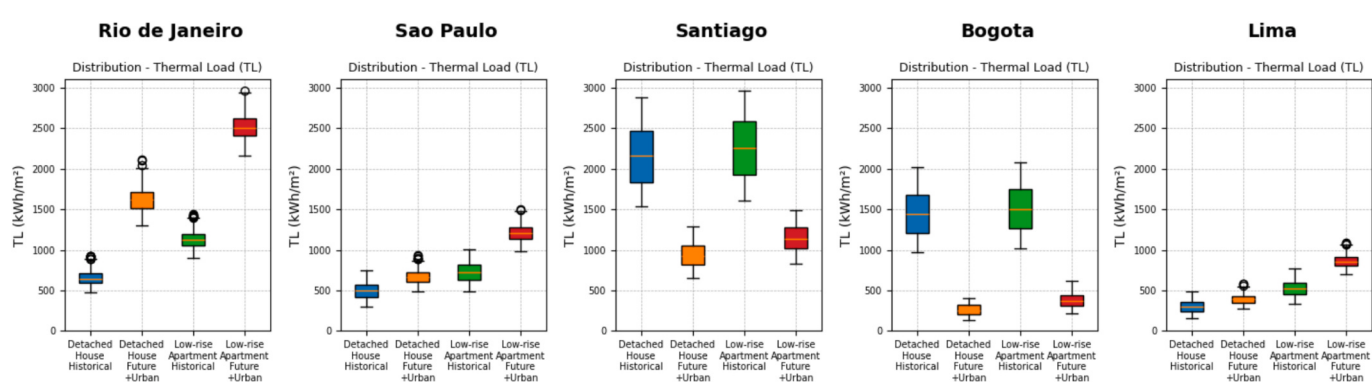


**Fig. 8.** Distribution of TL values for each dataset generated.

**Table 7**

Performance results across the source domain and target domain for each city.

City	Algorithm	Model	Source domain (Historical)			Target domain (Future)		
			R <sup>2</sup>	MAE	MAPE	R <sup>2</sup>	MAE	MAPE
Rio de Janeiro	XGBoost	Detached house	0.937	16	2	0.935	30	2
		Low-rise apartment	0.941	17	1	0.925	36	1
	ANN	Detached house	0.898	27	13	0.903	21	11
		Low-rise apartment	0.852	40	9	0.872	32	7
Sao Paulo	XGBoost	Detached house	0.985	9	2	0.910	20	3
		Low-rise apartment	0.981	12	2	0.934	21	2
	ANN	Detached house	0.930	21	25	0.810	30	15
		Low-rise apartment	0.914	27	18	0.832	34	9
Santiago	XGBoost	Detached house	0.998	12	1	0.978	17	2
		Low-rise apartment	0.998	12	1	0.980	18	2
	ANN	Detached house	0.985	40	22	0.960	25	19
		Low-rise apartment	0.963	42	22	0.960	27	17
Bogota	XGBoost	Detached house	0.998	10	1	0.967	9	4
		Low-rise apartment	0.998	10	1	0.934	17	5
	ANN	Detached house	0.986	29	25	0.869	22	33
		Low-rise apartment	0.977	37	23	0.871	26	27
Lima	XGBoost	Detached house	0.986	7	2	0.922	14	3
		Low-rise apartment	0.981	10	2	0.935	16	2
	ANN	Detached house	0.926	15	19	0.861	23	17
		Low-rise apartment	0.903	23	21	0.843	25	15

Overall, both algorithms consistently delivered R<sup>2</sup> values above 85 %, MAE below 40 kWh/m<sup>2</sup>, and MAPE below 30 % for the output. The transfer learning technique proved to be useful and effective as the initial hypothesis was validated in this initial step. In other words, the historical dataset successfully captured the relationship between input variables and output, and the smaller future urban dataset effectively reflected the shifts in TL driven by climate change. However, when transitioning from the source domain to the target domain, it was reported a slight decrease in performance metrics. Ultimately, XGBoost was chosen for the optimization phase because of its rapid training capabilities and ease of interpretation. In machine learning, an interpretable model enables humans to readily understand and explain their predictions or decisions. Although ANN delivered very similar results, it demands longer training periods and does not provide the same level of interpretability.

#### 4.3.2. Sensitivity analysis

The sensitivity analysis was performed using the SHAP method to highlight how climate change may change the input variables' importance, offering insights for the shifts in thermal-energy performance.

Fig. 9 illustrates the SHAP values for both architectural designs under different weather contexts.

SHAP values are interpreted as the contribution or the importance of each input variable to the model's prediction. In this discussion, positive SHAP values indicate that the input variable contributes to increasing the model's prediction relative to the baseline (average prediction), while negative values indicate that the variable contributes to decreasing the prediction. The hypothesis assumed that under the future urban context, the SHAP values would only vary in magnitudes, maintaining the same values, ranking, and priority of variables. However, in all cities, instances were observed where an input variable's impact shifted from positive to negative or vice versa. In other words, these results do not validate the initial hypothesis: because extreme conditions are absent from the historical record, the SHAP value dynamics diverge from the patterns observed under normal conditions. This indicated that climate change and UHI effects can significantly change the importance of input variables in the buildings' thermal-energy performance. Furthermore, these findings underscore the effectiveness of transfer learning in capturing shifts in thermal-energy performance, as the relationship between the input variables and the output adapts to

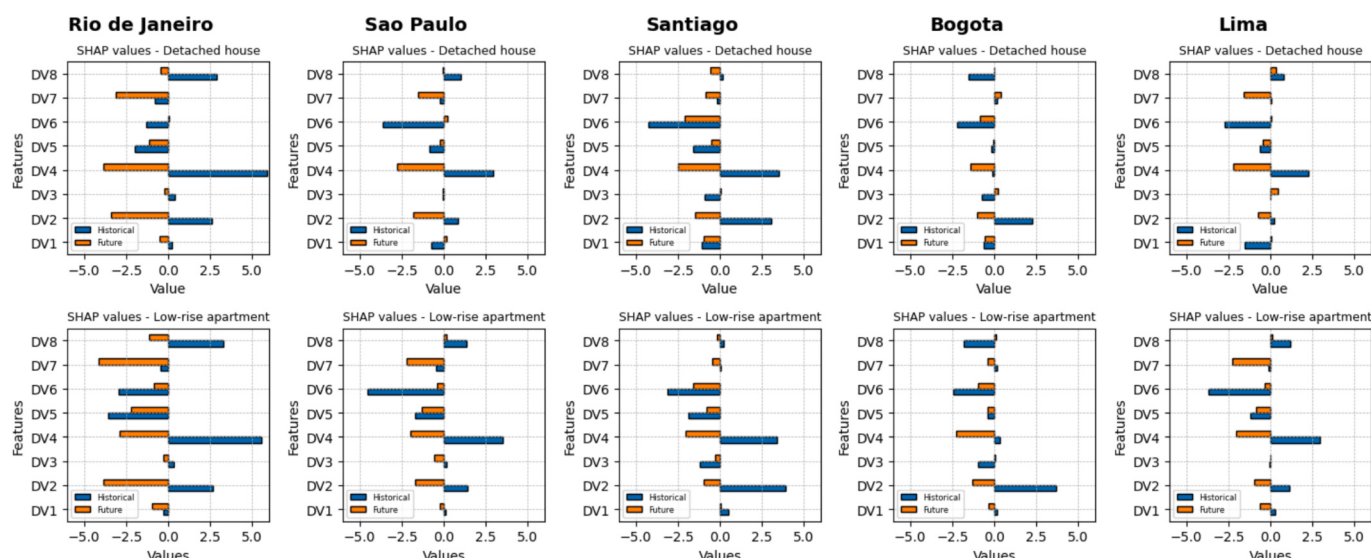


Fig. 9. SHAP values for each design variable for both architectural designs under historical and future urban weather contexts.

different weather contexts.

#### 4.4. Optimization results

This study optimized the building envelope based on the thermal-energy performance, carbon emissions, and total costs. Fig. 10 presents the Pareto front for each city under different weather contexts, with the respective architectural designs labeled. For a clear understanding of Fig. 10, the CE metric is displayed on the x-axis, the TL metric on the y-axis, and the TC metric is represented by the size of the dots.

As illustrated in Fig. 10, the Pareto fronts highlighted the impact of climate variations across the evaluated cities, with overlaps displayed in certain cases. For instance, in Sao Paulo and Lima, the Pareto front for detached houses under the future urban context coincided with the results for low-rise apartments under historical context. Similarly, in Santiago and Bogota, the Pareto front for detached houses under historical context overlapped with those for low-rise apartments under the same context. Finally, it is important to note that variations in the results are primarily driven by location and climate context, which directly affect the TC and TL metrics, as the CE metric remains constant across different locations.

#### 4.5. Decision-making process results

The final step focused on the decision-making process to identify the optimal solution. Fig. 11 illustrates the TOPSIS results for TL, CE, TC, and Equal weights preference contexts for both architectural models. To streamline the assessment process and focus on the study's primary objective—resilience to future urban weather conditions—only the future urban weather condition was presented and evaluated at this stage.

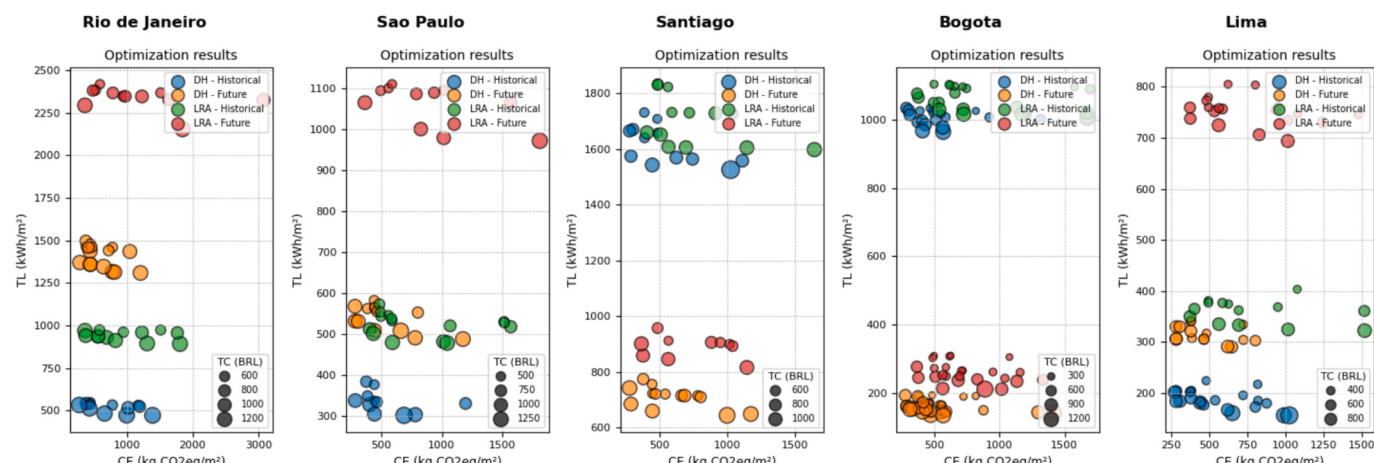
Fig. 11 highlights that when selecting the optimal solution based on a single metric causes significant scaling in the values of the other metrics. In other words, the optimal solution for the TL metric (lowest value) resulted in a significant increase in the values of the CE and TC metrics. This dynamic underscore the complexity of developing climate-resilient building designs, which require a holistic assessment. For instance, focusing only on thermal-energy performance may enhance adaptation but can lead to increased carbon emissions and total costs, thereby undermining mitigation efforts and potentially making the project economically unfeasible—and vice versa. Therefore, to evaluate the feasibility of climate-resilient building design, the Equal Weights context identifies solutions that prioritize all metrics equally.

For Rio de Janeiro, the TOPSIS solution under the Equal Weights context would increase the TL metric by 12 % and 11 %, the CE metric

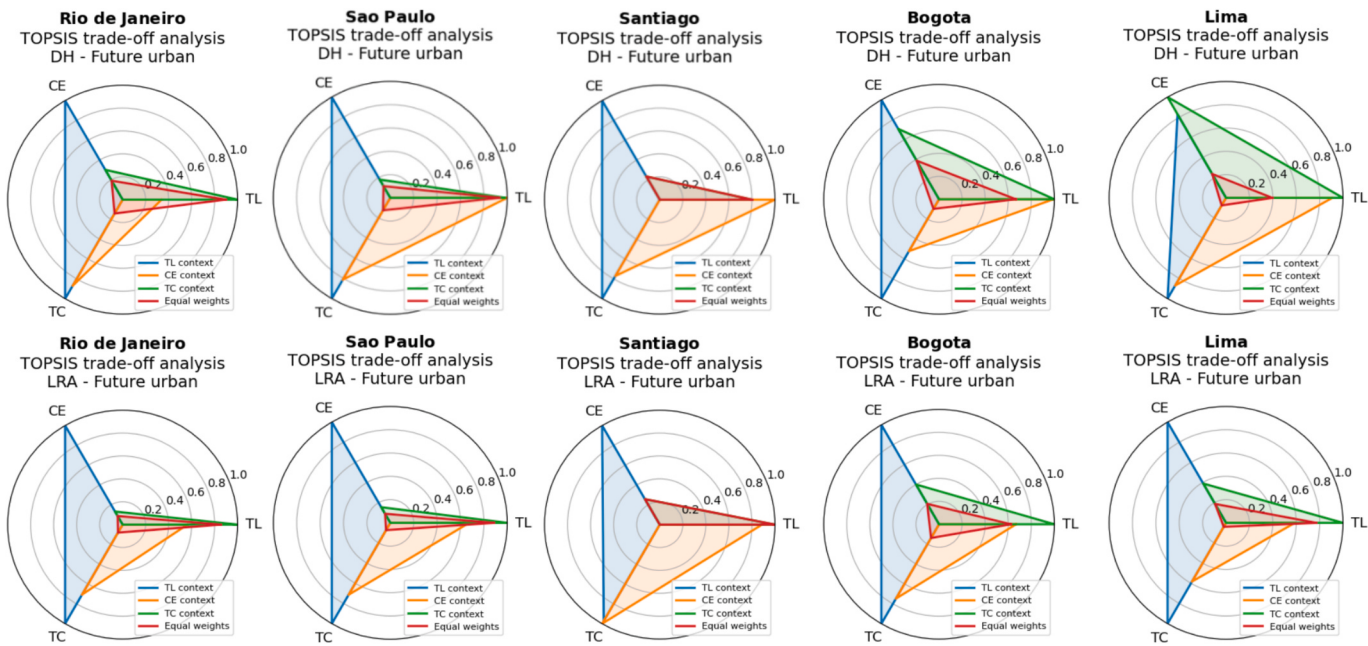
by 35 % and 44 %, and the TC metric by 17 % and 16 % for the DH and LRA, respectively. For Sao Paulo, the TL metric would increase by 15 % and 12 %, the CE metric by 35 % and 36 %, and the TC metric by 18 % and 13 % for the DH and LRA, respectively. In Santiago, the Equal Weights context would increase the TL metric by 12 % and 11 %, the CE metric by 61 % and 55 %, and no modifications in the TC metric for both DH and LRA, respectively. In Bogota, the Equal Weights context would increase the TL metric by 29 % and 28 %, the CE metric by 42 % and 36 %, and the TC metric by 36 % and 35 % for both DH and LRA, respectively. In Lima, the Equal Weights context would increase the TL metric by 6 % and 12 %, the CE metric by 36 % and 32 %, and the TC metric by 8 % and 7 % for both DH and LRA, respectively. Appendix A contains the complete list of optimal solutions for each context considered in each city. Finally, Table 8 illustrates the configurations of the optimal solutions selected through the TOPSIS method under the Equal Weights context.

Table 8 indicates that optimal configurations remain consistent across cities despite their distinct climate conditions. Constructive systems, such as traditional masonry, fiber cement or clay tiles with EPS boards for ceilings, and simple glazing, dominate the configuration settings. The primary difference lies in the variation of building orientation values, not only between cities but also among architectural models. Additionally, solutions derived from the TOPSIS method under the Equal Weight context revealed no differences among architectural models, such as wall, roof, ceiling, and glazing types remain largely uniform. Furthermore, the findings highlighted that future urban weather conditions necessitate small windows combined with low-absorptance values for the building envelope (walls and roofs) and insulated roof to enhance thermal performance. Lastly, while new and advanced construction systems available on the market could improve adaptation and mitigation to future urban climates, their feasibility is limited by cost and carbon emissions. The optimization results indicated that climate resilience is best accomplished through architectural passive design. A design that prioritizes solar orientation to enhance thermal performance, combined with moderately sized windows, light-colored walls and roofs, and insulated roof offers a cost-effective approach while promoting more sustainable and equitable solutions.

Finally, a brief analysis was conducted to compare the variation in optimal designs across different climate contexts. To keep the discussion concise, Appendix A presents the configurations of the optimal solutions identified using the TOPSIS method under Equal Weights and historical climate contexts. While the configurations for both models are largely consistent, particularly regarding wall type, glazing type, and WWR, some location-specific differences emerged. In Rio de Janeiro and Lima, future urban weather conditions prompted the inclusion of roof insulation. Conversely, Sao Paulo, Santiago, and Bogota exhibited a shift



**Fig. 10.** Pareto front results from each optimization for both architectural designs under historical and future urban weather contexts.



**Fig. 11.** TOPSIS trade-off analysis for both architectural designs under future urban weather context.

**Table 8**

TOPSIS optimal solutions settings under the Equal Weights context for future urban weather context.

City	Model	Orientation	Wall type	Roof type	Ceiling type	Glazing type	WWR	Absorptance value – Wall	Absorptance value – Roof
Rio de Janeiro	Detached house	270	W1	R2	C5	G1	20	0.2	0.2
	Low-rise apartment	135	W1	R1	C5	G1	20	0.2	0.2
Sao Paulo	Detached house	90	W1	R2	C5	G1	20	0.2	0.3
	Low-rise apartment	90	W1	R2	C5	G1	20	0.2	0.3
Santiago	Detached house	270	W1	R2	C5	G1	20	0.2	0.3
	Low-rise apartment	135	W1	R1	C5	G1	20	0.2	0.2
Bogota	Detached house	45	W1	R2	C5	G1	20	0.3	0.3
	Low-rise apartment	90	W1	R1	C5	G1	20	0.2	0.2
Lima	Detached house	270	W1	R1	C5	G1	20	0.2	0.2
	Low-rise apartment	180	W1	R1	C5	G1	20	0.3	0.2

toward lower absorptance values for the envelope to reduce heat gains. Under the historical weather conditions, where insulated walls are more costly, the optimal designs in Santiago, Bogota, and Sao Paulo instead favored higher absorptance to harness solar gains. Thus, the primary design shift from historical to future urban weather contexts involves adopting roof insulation in Rio de Janeiro and Lima, and reducing absorptance values in Sao Paulo, Santiago, and Bogota.

## 5. Discussion

To address the uncertainty of climate change, this study distinguished from others [29–34] by incorporating the latest emissions scenario (SSP5-8.5 from the AR6) combined with UHI effects to generate hypothetical future urban weather datasets. As demonstrated in previous studies [70,112,113], accounting for the diverse climates across multiple locations is an effective and comprehensive strategy. Because

this approach essentially allows for a broader assessment of technical solutions, showcasing its adaptability and potential for different conditions. Consequently, BPS tools play a crucial role in overcoming experimental constraints, particularly when addressing complex and uncertain challenges such as climate change [19].

From a machine learning perspective, the models developed for predicting TL in the evaluated cities achieved performance levels comparable to those reported in the literature [48], with  $R^2$  values exceeding 85 % for both XGBoost and ANN. Additionally, this study leveraged transfer learning to improve computational efficiency—a technique still underutilized in the building performance field [56]. While previous research has highlighted the limitations of transfer learning when applied to multiple building types—particularly as performance deteriorates with significant variations in design parameters or performance objectives [55]—this study demonstrated its viability and efficiency. Although SHAP analysis revealed that climate change and

UHI effects can substantially alter the influence of input variables on a building's thermal-energy performance. The transfer learning results showed that the technique was able to adapt to different climate conditions. Lastly, though rarely explored in the literature [56,57], integrating machine learning and optimization algorithms offer significant advantages such as reducing computational and simulation demands and facilitating the evaluation of technologies, construction materials, and design solutions more efficiently [58,59].

While multi-criteria decision-making techniques are ideal for selecting the optimal solution, many studies focus on analyzing the Pareto front settings [48]. Therefore, following previous studies [61,62], the TOPSIS method was chosen ensuring that trade-offs lead to solutions that are both sustainable and equitable. Although numerous studies highlight the thermal performance benefits of new construction systems such as ICF, SCIP, Steel and Wood Frame systems [88–91], their feasibility remains limited for vulnerable communities due to cost and carbon emission constraints. Because obtaining accurate labor-cost data proved challenging, we did not include it in this study; this omission further underscores the cost constraints of new construction systems. Therefore, by evaluating thermal performance, carbon emissions, and total costs, the TOPSIS analysis indicated that achieving climate resilience in Latin America is best accomplished through architectural passive design, a conclusion also reported in other studies [44–47]. The optimal solution typically combines conventional construction practices with passive design strategies, such as optimal solar orientation, moderate window sizing, and low-absorptance values for the building envelope (walls and roofs) and insulated roof. However, this presents a significant challenge for industry and society in general because high-quality architectural design is often viewed as subjective and associated with high costs, making it less accessible to vulnerable communities. Although public policies can incentivize more affordable and efficient construction systems, quality of design remains a persistent issue. Governments frequently address the housing deficit by implementing standardized social housing prototypes [45]. Therefore, this one-size-fits-all approach should be replaced with passive design solutions that can tackle future urban climate challenges in Latin America [113–121]. More specifically, developing climate-resilient design guidelines for the Global South through simulations based on future urban climate data presents a promising approach to address this challenge.

## 6. Conclusion

This study explored the feasibility of climate-resilient building design in the residential sector of the Global South. Specifically, a simulation-based analysis was conducted across five major urban Latin America centers—Rio de Janeiro and Sao Paulo (Brazil), Santiago (Chile), Bogota (Colombia), and Lima (Peru)—chosen for their rapid urbanization, persistent housing shortages, and climate diversity.

In the first step, this study generated hypothetical future urban weather files by integrating IPCC emissions scenarios with urban heat island effects. The results showed future urban conditions trending towards higher DBT, RH, and GHR by 2080. The average DBT difference between historical and future climates was up to 3 °C across all cities. However, this difference rose up to 6 °C with the inclusion of the UHI effects. These findings underscore the importance of creating future urban climate models that can inform the development for climate-resilient building design.

In the second step, XGBoost and ANN were considered for surrogate modeling, combined with the transfer learning technique. In addition, the SHAP method was used to evaluate how climate change influences the importance of input variables. Both algorithms yielded accurate results, achieving  $R^2$  values above 85 %, MAE values below 40 kWh/m<sup>2</sup>, and MAPE values below 30 %. The SHAP values indicated that climate change and urban heat island effects can substantially modify the buildings' thermal-energy performance dynamics. These findings

highlighted the effectiveness of transfer learning in capturing buildings' thermal-energy performance changes under varying weather conditions.

In the third step, these surrogate models were coupled with the NSGA-III to optimize the building envelope based on thermal-energy performance, carbon emissions, and total costs. Lastly, the TOPSIS method was used to perform the trade-off analysis, with different weighting factors for each metric, depending on the preference context. In general, when selecting the optimal solution based on a single metric causes significant scaling in the value of the other metrics. To assess the feasibility of climate-resilient building design, the Equal Weights context was established to ensure that all metrics were equally prioritized. Overall, the TOPSIS Equal Weights context solution indicated increases up to 12 % in thermal load, 61 % in carbon emissions, and 36 % in total costs, depending on the city analyzed. Despite climate variations, the optimal building envelope configurations remained consistent across different cities. Although new and advanced construction systems, such as ICF/SCIP walls and steel/wood frame systems, could enhance adaptation and mitigation to future climates, their feasibility remains constrained by cost and carbon emissions. Therefore, this study concluded that climate-resilient building design in Latin America is best attained through passive architectural strategies. A good solar orientation, small windows, light-colored envelopes, and insulated roof provided a cost-effective, sustainable, and equitable solution to protect vulnerable communities in the Global South.

Finally, when looking ahead, several aspects need further investigation. Future research should expand the cost assessment to encompass all building components and labor costs; evaluate different occupancy patterns to identify it affects the optimal building design; explore different weighting schemes in the decision-making process; consider additional environmental metrics and environmental impact from the transportation of materials and the building's operational phase; evaluate different and realistic urban morphologies in detail during heat island modeling; explore different ventilation strategies, replicate the proposed method to other building typologies such as commercial facilities, and investigate the potential of shading devices.

## Ethical approval

This study does not contain any studies with human or animal subjects performed by any of the authors.

## Declaration of Generative AI and AI-assisted technologies in the writing process

During the preparation of this work the authors used ChatGPT to address grammar issues and enhance readability. After using this tool/service, the authors reviewed and edited the content as needed and took full responsibility for the content of the published article.

## CRediT authorship contribution statement

**Alexandre Santana Cruz:** Writing – review & editing, Writing – original draft, Visualization, Software, Methodology, Investigation, Conceptualization. **Rafael Eduardo López-Guerrero:** Writing – review & editing, Software, Methodology, Investigation. **Vítor Freitas Mendes:** Writing – review & editing. **Leopoldo Eurico Gonçalves Bastos:** Writing – review & editing, Supervision. **Lucas Rosse Caldas:** Writing – review & editing, Supervision.

## Declaration of competing interest

The authors declare that they have no known competing financial interests or personal relationships that could have appeared to influence the work reported in this paper.

## Acknowledgments

This study was supported by the Brazilian Federal Agency for the Support and Evaluation of Graduate Education - Brazil (CAPES) -

Financing Code 001. Fundação Carlos Chagas Filho de Amparo à Pesquisa do Estado do Rio de Janeiro (FAPERJ), E-26/200.162/2023 (281990).

## Appendix A. Material takeoff for architectural designs and carbon emission indexes

**Table A1** details the surface areas (in square meters) of each envelope system for both the detached house and low-rise apartment. **Table A2** lists the materials comprising the construction systems explored in this study, along with their respective carbon emission values and units. **Table A3** contains the complete list of optimal solutions for each context considered in each city. Finally, **Table A4** lists the TOPSIS optimal solutions settings under the Equal Weights and historical weather contexts.

**Table A1**

Surface areas of each envelope system.

Take-off in square meters ( $m^2$ )

Index	Envelope system	Detached house	Low-rise apartment
1	Wall	120	160
2	Roof	78	120
3	Ceiling	56	62
4	Glazing: 20 % WWR	9	9
5	Glazing: 30 % WWR	14	14
6	Glazing: 40 % WWR	19	19
7	Glazing: 50 % WWR	23	23
8	Glazing: 60 % WWR	28	28

**Table A2**

List of materials used with their respective carbon emission values.

Carbon emission indexes

Index	List of material	kgCO <sub>2</sub> -eq	Unit
1	Coating mortar	412.7	$m^3$
2	Ceramic blocks	0.15	kg
3	Concrete blocks	0.11	kg
4	Concrete	254.7	$m^3$
5	EPS board	4.8	kg
6	Cement board	1.2	kg
7	OSB board	-662	$m^3$
8	Rock wool	1.3	kg
9	Fiber cement tiles	0.83	kg
10	Clay tiles	0.89	unit
11	Metal tiles	3.03	kg
12	Plaster panel	0.33	kg
13	Wooden lining	-5.4	$m^2$
14	PVC board	3.1	kg
15	Simple glazing	29	$m^2$
16	Double panel glazing	65	$m^2$
17	Triple panel glazing	105	$m^2$

**Table A3**

List of optimal solutions for each context considered in each city under future urban weather scenario.

City	Context	Model	Orientation	Wall type	Roof type	Ceiling type	Glazing type	WWR	Absorptance value – Wall	Absorptance value – Roof
Rio de Janeiro	TL	DH	270	W5	R1	C5	G3	20	0.3	0.2
	CE		270	W7	R1	C5	G1	20	0.2	0.2
	TC		225	W3	R1	C5	G1	20	0.2	0.2
	Equal Weights		270	W1	R2	C5	G1	20	0.2	0.2
	TL	LRA	0	W5	R1	C5	G3	20	0.3	0.5
	CE		0	W7	R2	C2	G1	20	0.3	0.2
	TC		135	W3	R1	C5	G1	20	0.2	0.2
	Equal Weights		135	W1	R1	C5	G1	20	0.2	0.2
Sao Paulo	TL	DH	315	W4	R3	C5	G3	20	0.2	0.5

(continued on next page)

**Table A3 (continued)**

City	Context	Model	Orientation	Wall type	Roof type	Ceiling type	Glazing type	WWR	Absorptance value – Wall	Absorptance value – Roof
Santiago	CE	LRA	180	W7	R1	C1	G1	20	0.2	0.2
	TC		90	W3	R1	C5	G1	20	0.2	0.3
	Equal Weights		90	W1	R2	C5	G1	20	0.2	0.3
	TL		45	W4	R3	C5	G2	20	0.2	0.7
	CE		0	W7	R2	C2	G1	20	0.2	0.2
	TC	LRA	90	W3	R1	C3	G1	20	0.2	0.2
	Equal Weights		90	W1	R2	C5	G1	20	0.2	0.2
	TL		225	W4	R2	C5	G3	20	0.2	0.2
	CE		225	W7	R1	C5	G1	20	0.3	0.2
	TC		270	W1	R4	C1	G1	20	0.2	0.2
	Equal Weights		270	W1	R2	C5	G1	20	0.2	0.2
	TL	LRA	135	W4	R3	C5	G2	20	0.3	0.7
	CE		135	W7	R4	C2	G1	20	0.2	0.2
	TC		135	W1	R4	C1	G1	20	0.3	0.2
	Equal Weights		135	W1	R2	C5	G1	20	0.2	0.2
	TL		180	W4	R4	C4	G1	20	0.6	0.8
	CE	LRA	0	W7	R2	C2	G1	20	0.8	0.2
	TC		0	W1	R4	C1	G1	20	0.7	0.4
	Equal Weights		45	W1	R1	C5	G1	20	0.7	0.4
	TL		0	W4	R1	C5	G2	20	0.8	0.5
	CE		0	W7	R2	C2	G1	20	0.8	0.2
	TC	LRA	90	W1	R4	C1	G1	20	0.3	0.5
	Equal Weights		90	W1	R1	C5	G1	20	0.3	0.5
	TL		270	W6	R1	C5	G2	20	0.2	0.2
	CE		0	W7	R1	C1	G1	20	0.2	0.2
	TC		270	W1	R1	C1	G2	20	0.2	0.2
	Equal Weights		270	W1	R1	C5	G1	20	0.2	0.2
	TL	LRA	180	W4	R2	C5	G2	20	0.5	0.3
	CE		180	W7	R1	C1	G1	20	0.3	0.2
	TC		180	W1	R4	C1	G1	20	0.2	0.2
	Equal Weights		180	W1	R1	C5	G1	20	0.3	0.2

**Table A4**

TOPSIS optimal solutions settings under the Equal Weights context for historical weather context.

City	Model	Orientation	Wall type	Roof type	Ceiling type	Glazing type	WWR	Absorptance value – Wall	Absorptance value – Roof
Rio de Janeiro	Detached house	270	W1	R1	C1	G1	20	0.2	0.2
	Low-rise apartment	315	W1	R1	C1	G1	20	0.2	0.2
Sao Paulo	Detached house	225	W1	R1	C5	G1	20	0.2	0.7
	Low-rise apartment	270	W1	R1	C5	G1	20	0.2	0.7
Santiago	Detached house	180	W1	R1	C5	G1	20	0.8	0.8
	Low-rise apartment	270	W1	R1	C5	G1	20	0.7	0.8
Bogota	Detached house	225	W1	R1	C1	G1	20	0.8	0.8
	Low-rise apartment	45	W1	R1	C1	G1	20	0.8	0.6
Lima	Detached house	180	W1	R1	C1	G1	20	0.3	0.5
	Low-rise apartment	135	W1	R1	C1	G1	20	0.2	0.5

## Data availability

Data will be made available on request.

## References

- [1] N. Dados, R. Connell, The Global South, *Contexts* 11 (2012) 12–13, <https://doi.org/10.1177/1536504212436479>.
- [2] IPCC, Intergovernmental Panel on Climate Change: Climate Change AR1 Synthesis Report, 1990.
- [3] IPCC, Intergovernmental Panel on Climate Change: Climate Change AR2 Synthesis Report, 1995.
- [4] IPCC, Climate Change AR3 Synthesis Report, 2001.
- [5] IPCC, Intergovernmental Panel on Climate Change: Climate Change AR4 Synthesis Report, 2007.
- [6] IPCC, Intergovernmental Panel on Climate Change: Climate Change AR5 Synthesis Report, 2014.
- [7] IPCC, Intergovernmental Panel on Climate Change: Climate Change AR6 Synthesis Report, 2023. <https://doi.org/10.59327/IPCC/AR6-9789291691647>.
- [8] IEA, The Future of Cooling Opportunities for Energy-Efficient Air-Conditioning Together Secure Sustainable, n.d. [www.iea.org/t&c/](http://www.iea.org/t&c/).
- [9] IEA, The Future of Cooling Opportunities for energy-efficient air conditioning Together Secure Sustainable, International Energy Agency (2018). <https://doi.org/10.1787/9789264301993>.
- [10] IEA, World Energy Balances 2022, International Energy Agency – (2022) 1–23. <https://doi.org/10.1787/data-00512-en>.
- [11] World Bank, Economic Review: Latin America and the Caribbean, 2024. <https://doi.org/10.1596/978-1-4648-2182-0>.
- [12] R. Lubbock, E. Vivas, The reconfiguration of twenty-first century Latin American regionalism: actors, processes, contradictions, and prospects, *Globalizations* 19 (2022) 519–535, <https://doi.org/10.1080/14747731.2021.2011588>.
- [13] OECD, Latin American Economic Outlook 2023, OECD, 2015.
- [14] L.S. Wainer, Resilient solutions to reduce the housing deficit in Latin America and the Caribbean, Washington, D.C., 2022. <https://doi.org/10.18235/0004465>.
- [15] L. Marín-Restrepo, A. Pérez, F. María, B. Piderit-Moreno, M. Trebilcock-Kelly, P. Wegterseder-Martínez Editors, Removing Barriers to Environmental Comfort in the Global South, Springer International Publishing, Cham, 2023.
- [16] T. Vigevani, H. Ramazini Junior, The Challenges for Building Regional Integration in the Global South, Springer International Publishing, Cham, 2022.
- [17] UN, Envisaging the Future of Cities, 2022. [https://unhabitat.org/sites/default/files/2022/06/wcr\\_2022.pdf](https://unhabitat.org/sites/default/files/2022/06/wcr_2022.pdf) (accessed June 26, 2024).
- [18] UN, Global Sustainable Development Report 2023, 2023. [https://sdgs.un.org/sites/default/files/2023-09/FINAL%20GSDR%202023-Digital%20-110923\\_1.pdf](https://sdgs.un.org/sites/default/files/2023-09/FINAL%20GSDR%202023-Digital%20-110923_1.pdf) (accessed June 26, 2024).
- [19] A.S. Cruz, V.F. Mendes, J.C. Mendes, L.R. Caldas, L.E. Gonçalves Bastos, What lies ahead? The future performance of Global South residential buildings amid climate change: a systematic literature review, *J. Build Eng* 98 (2024) 111486, <https://doi.org/10.1016/j.jobe.2024.111486>.
- [20] T. Kesik, W. O'Brien, A. Ozkan, Toward a standardized framework for thermal resilience modelling and its practical application to futureproofing, *Sci. Technol. Built Environ.* 28 (2022) 742–756, <https://doi.org/10.1080/23744731.2022.2043069>.
- [21] S. Homaei, M. Hamdy, Thermal resilient buildings: how to be quantified? A novel benchmarking framework and labelling metric, *Build. Environ.* 201 (2021), <https://doi.org/10.1016/j.buildenv.2021.108022>.
- [22] S. Attia, R. Levinson, E. Ndongo, P. Holzer, O. Berk Kazancı, S. Homaei, C. Zhang, B.W. Olesen, D. Qi, M. Hamdy, P. Heiselberg, Resilient cooling of buildings to protect against heat waves and power outages: key concepts and definition, *Energ. Build.* 239 (2021), <https://doi.org/10.1016/j.enbuild.2021.110869>.
- [23] W. Miller, A. Machard, E. Bozomnet, N. Yoon, D. Qi, C. Zhang, A. Liu, A. Sengupta, J. Akander, A. Hayati, M. Cehlin, O.B. Kazancı, R. Levinson, Conceptualising a resilient cooling system: a socio-technical approach, *City Environ. Interact.* 11 (2021), <https://doi.org/10.1016/j.cacint.2021.100065>.
- [24] D.B. Crawley, L.K. Lawrie, Should we be using just “typical” weather data in building performance simulation?, in: Building Simulation Conference Proceedings, International Building Performance Simulation Association, 2019: pp. 4801–4808. <https://doi.org/10.26868/25222708.2019.210594>.
- [25] A. Machard, C. Inard, J.M. Alessandrini, C. Pelé, J. Ribéron, A Methodology for assembling future weather files including heatwaves for building thermal simulations from the European Coordinated Regional Downscaling Experiment (EURO-CORDEX) climate data, *Energies (Basel)* 13 (2020), <https://doi.org/10.3390/en13133424>.
- [26] R. Cole, R. Evans, M. Eames, An empirical review of methods to assess overheating in buildings in the context of changes to extreme heat events, *J. Build. Perform. Simul.* 17 (2024) 322–337, <https://doi.org/10.1080/19401493.2023.2276711>.
- [27] R. Escandón, C.M. Calama-González, A. Alonso, R. Suárez, A.L. León-Rodríguez, How do different methods for generating future weather data affect building performance simulations? A comparative analysis of Southern Europe, *Buildings* 13 (2023), <https://doi.org/10.3390/buildings13092385>.
- [28] E. Rodrigues, M.S. Fernandes, D. Carvalho, Future weather generator for building performance research: an open-source morphing tool and an application, *Build. Environ.* 233 (2023), <https://doi.org/10.1016/j.buildenv.2023.110104>.
- [29] J.M. Hugo, Heat stress: adaptation measures in South African informal settlements, *Build. Cities* 4 (2023) 55–73, <https://doi.org/10.5334/bc.269>.
- [30] J. Xiong, S. Guo, Y. Wu, D. Yan, C. Xiao, X. Lu, Predicting the response of heating and cooling demands of residential buildings with various thermal performances in China to climate change, *Energy* 269 (2023), <https://doi.org/10.1016/j.energy.2023.126789>.
- [31] K. Verichev, M. Zamorano, M. Carpio, Effects of climate change on variations in climatic zones and heating energy consumption of residential buildings in the southern Chile, *Energ. Build.* 215 (2020), <https://doi.org/10.1016/j.enbuild.2020.109874>.
- [32] I.J.A. Callejas, R.M. Apolonio, E.L.A. da Guarda, L.C. Durante, K. de A.C. Rossetti, F. Roseta, L.M. Do Amarante, Bermed earth-sheltered wall for low-income house: thermal and energy measure to face climate change in tropical region, *Appl. Sci. (Switzerland)* 11 (2021) 1–22, <https://doi.org/10.3390/app11010420>.
- [33] A.C. Borbon-Almada, J. Lucero-Alvarez, N.A. Rodriguez-Muñoz, M. Ramirez-Celaya, S. Castro-Brockman, N. Sau-Soto, M. Najera-Trejo, Design and application of cellular concrete on a Mexican residential building and its influence on energy savings in hot climates: projections to 2050, *Appl. Sci. (Switzerland)* 10 (2020) 1–22, <https://doi.org/10.3390/app10228225>.
- [34] A. Dodoo, J. Ayarkwa, Effects of climate change for thermal comfort and energy performance of residential buildings in a Sub-Saharan African climate, *Buildings* 9 (2019), <https://doi.org/10.3390/buildings9100215>.
- [35] K. Verichev, M. Zamorano, A. Fuentes-Sepúlveda, N. Cárdenas, M. Carpio, Adaptation and mitigation to climate change of envelope wall thermal insulation of residential buildings in a temperate oceanic climate, *Energ. Buildings* 235 (2021), <https://doi.org/10.1016/j.enbuild.2021.110719>.
- [36] A. Kamal, A. Mahfouz, N. Sezer, I.G. Hassan, L.L. Wang, M.A. Rahman, Investigation of urban heat island and climate change and their combined impact on building cooling demand in the hot and humid climate of Qatar, *Urban Clim.* 52 (2023), <https://doi.org/10.1016/j.uclim.2023.101704>.
- [37] M. Palme, L. Inostroza, G. Villares, A. Lobato-Cordero, C. Carrasco, From urban climate to energy consumption. Enhancing building performance simulation by including the urban heat island effect, *Energ. Build.* 145 (2017) 107–120, <https://doi.org/10.1016/j.enbuild.2017.03.069>.
- [38] J. Litardo, M. Palme, M. Borbor-Cordova, R. Caiza, J. Macias, R. Hidalgo-Leon, G. Soriano, Urban Heat Island intensity and buildings' energy needs in Duran, Ecuador: simulation studies and proposal of mitigation strategies, *Sustain. Cities Soc.* 62 (2020), <https://doi.org/10.1016/j.scs.2020.102387>.
- [39] Y. Liu, R. Stouffs, A. Tablada, N.H. Wong, J. Zhang, Comparing micro-scale weather data to building energy consumption in Singapore, *Energ. Build.* 152 (2017) 776–791, <https://doi.org/10.1016/j.enbuild.2016.11.019>.
- [40] Y.X. Ma, A.C. Yu, Impact of urban heat island on high-rise residential building cooling energy demand in Hong Kong, *Energ. Build.* 311 (2024), <https://doi.org/10.1016/j.enbuild.2024.114127>.
- [41] I. Lima, V. Scalco, R. Lamberts, Estimating the impact of urban densification on high-rise office building cooling loads in a hot and humid climate, *Energ. Build.* 182 (2019) 30–44, <https://doi.org/10.1016/j.enbuild.2018.10.019>.
- [42] P. Kumari, S. Kapur, V. Garg, K. Kumar, Effect of surface temperature on energy consumption in a calibrated building: a case study of Delhi, *Climate* 8 (2020), <https://doi.org/10.3390/CL18060071>.
- [43] R. Andersen, K. Negendahl, Lifespan prediction of existing building typologies, *J. Build. Eng.* 65 (2023), <https://doi.org/10.1016/j.jobe.2022.105696>.
- [44] J. Gamero-Salinas, A. Monge-Barrio, N. Krishnani, J. López-Fidalgo, A. Sánchez-Ostiz, Passive cooling design strategies as adaptation measures for lowering the indoor overheating risk in tropical climates, *Energ. Build.* 252 (2021), <https://doi.org/10.1016/j.enbuild.2021.111417>.
- [45] S. Flores-Larsen, C. Filippin, G. Barea, Impact of climate change on energy use and bioclimatic design of residential buildings in the 21st century in Argentina, *Energ. Buildings* 184 (2019) 216–229, <https://doi.org/10.1016/j.enbuild.2018.12.015>.
- [46] E.L.S. Gonçalves, J.L. Braga, A. de O. Sampaio, V. dos S. Batista, L.J. da R. Menezes, L.G. Eli, M.S. Barata, R. da S. Ventura Neto, B.R. Zemero, Multiscale modeling to optimize thermal performance design for urban social housing: A case study, *Appl. Therm. Eng.* 236 (2024). <https://doi.org/10.1016/j.applthermaleng.2023.121379>.
- [47] A.F. Krelling, R. Lamberts, J. Malik, W. Zhang, K. Sun, T. Hong, Defining weather scenarios for simulation-based assessment of thermal resilience of buildings under current and future climates: a case study in Brazil, *Sustain. Cities Soc.* 107 (2024), <https://doi.org/10.1016/j.scs.2024.105460>.
- [48] A.S. Cruz, L.R. Caldas, V.M. Mendes, J.C. Mendes, L.E.G. Bastos, Multi-objective optimization based on surrogate models for sustainable building design: a systematic literature review, *Build. Environ.* 266 (2024), <https://doi.org/10.1016/j.buildenv.2024.112147>.
- [49] P. Westermann, R. Evans, Surrogate modelling for sustainable building design – a review, *Energ. Build.* 198 (2019) 170–186, <https://doi.org/10.1016/j.enbuild.2019.05.057>.
- [50] Z. Wang, R.S. Srinivasan, A review of artificial intelligence based building energy use prediction: contrasting the capabilities of single and ensemble prediction models, *Renew. Sustain. Energy Rev.* 75 (2017) 796–808, <https://doi.org/10.1016/j.rser.2016.10.079>.
- [51] Y. Sun, F. Haghhighat, B.C.M. Fung, A review of the-state-of-the-art in data-driven approaches for building energy prediction, *Energ. Buildings* 221 (2020) 11022, <https://doi.org/10.1016/j.enbuild.2020.110022>.
- [52] K. Amasyali, N.M. El-Gohary, A review of data-driven building energy consumption prediction studies, *Renew. Sustain. Energy Rev.* 81 (2018) 1192–1205, <https://doi.org/10.1016/j.rser.2017.04.095>.

- [53] Y. Zou, S. Lou, D. Xia, I.Y.F. Lun, J. Yin, Multi-objective building design optimization considering the effects of long-term climate change, *J. Build. Eng.* 44 (2021) 102904, <https://doi.org/10.1016/j.jobe.2021.102904>.
- [54] Z. Li, Y. Zhao, H. Xia, S. Xie, A multi-objective optimization framework for building performance under climate change, *J. Build. Eng.* 80 (2023), <https://doi.org/10.1016/j.jobe.2023.107978>.
- [55] H. Yan, G. Ji, K. Yan, Data-driven prediction and optimization of residential building performance in Singapore considering the impact of climate change, *Build. Environ.* 226 (2022), <https://doi.org/10.1016/j.buildenv.2022.109735>.
- [56] Y.-D. Ko, C.-S. Park, Parameter estimation of unknown properties using transfer learning from virtual to existing buildings, *J. Build. Perform. Simul.* 14 (2021) 503–514, <https://doi.org/10.1080/19401493.2021.1972159>.
- [57] A. Hosna, E. Merry, J. Gyalmo, Z. Alom, Z. Aung, M.A. Azim, Transfer learning: a friendly introduction, *J Big Data* 9 (2022) 102, <https://doi.org/10.1186/s40537-022-00652-w>.
- [58] M. Lagunas, B. Impata, V. Martinez, V. Fernandez, C. Georgakis, S. Braun, F. Bertrand, Transfer learning for fine-grained classification using semi-supervised learning and visual transformers, (2023). <http://arxiv.org/abs/2305.10018>.
- [59] S.J. Pan, Q. Yang, A survey on transfer learning, *IEEE Trans. Knowl. Data Eng.* 22 (2010) 1345–1359, <https://doi.org/10.1109/TKDE.2009.191>.
- [60] R. Wang, S. Lu, W. Feng, A three-stage optimization methodology for envelope design of passive house considering energy demand, thermal comfort and cost, *Energy* 192 (2020) 116723, <https://doi.org/10.1016/j.energy.2019.116723>.
- [61] S. Mohammad, E. Saryazdi, A. Etemad, A. Shafaat, A.M. Bahman, Data-driven performance analysis of a residential building applying artificial neural network (ANN) and multi-objective genetic algorithm (GA), *Build Environ.* 225 (2022) 109633, <https://doi.org/10.1016/j.buildenv.2022.109633>.
- [62] J. Song, W. Wang, P. Ni, H. Zheng, Z. Zhang, Y. Zhou, Framework on low-carbon retrofit of rural residential buildings in arid areas of northwest China: a case study of Turpan residential buildings, *Build. Simul.* 16 (2023) 279–297, <https://doi.org/10.1007/s12273-022-0941-9>.
- [63] R. Chen, Y.S. Tsay, T. Zhang, A multi-objective optimization strategy for building carbon emission from the whole life cycle perspective, *Energy* 262 (2023) 125373, <https://doi.org/10.1016/j.energy.2022.125373>.
- [64] R. Chen, Y.S. Tsay, S. Ni, An integrated framework for multi-objective optimization of building performance: Carbon emissions, thermal comfort, and global cost, *J. Clean. Prod.* 359 (2022) 131978, <https://doi.org/10.1016/j.jclepro.2022.131978>.
- [65] E.M. Hamin, N. Curran, Urban form and climate change: balancing adaptation and mitigation in the U.S. and Australia, *Habitat. Int.* 33 (2009) 238–245, <https://doi.org/10.1016/j.habitatint.2008.10.005>.
- [66] L. Xu, X. Wang, J. Liu, Y. He, J. Tang, M. Nguyen, S. Cui, Identifying the trade-offs between climate change mitigation and adaptation in urban land use planning: an empirical study in a coastal city, *Environ. Int.* 133 (2019), <https://doi.org/10.1016/j.envint.2019.105162>.
- [67] climate.onebuilding.org, (n.d.). <https://climate.onebuilding.org/> (accessed November 8, 2024).
- [68] L.M. Campagna, F. Fiorito, On the impact of climate change on building energy consumptions: a meta-analysis, *Energies (Basel)* 15 (2022), <https://doi.org/10.3390/en15010354>.
- [69] V. Eyring, S. Bony, G.A. Meehl, C.A. Senior, B. Stevens, R.J. Stouffer, K.E. Taylor, Overview of the coupled model intercomparison project phase 6 (CMIP6) experimental design and organization, *Geosci. Model Dev.* 9 (2016) 1937–1958, <https://doi.org/10.5194/gmd-9-1937-2016>.
- [70] M.K. Bracht, M.S. Olinger, A.F. Krelling, A.R. Gonçalves, A.P. Melo, R. Lamberts, Multiple regional climate model projections to assess building thermal performance in Brazil: understanding the uncertainty, *J. Build. Eng.* 88 (2024), <https://doi.org/10.1016/j.jobe.2024.109248>.
- [71] B. Bueno, M. Roth, L. Norford, R. Li, Computationally efficient prediction of canopy level urban air temperature at the neighbourhood scale, *Urban Clim.* 9 (2014) 35–53, <https://doi.org/10.1016/j.uclim.2014.05.005>.
- [72] J. Mao, J.H. Yang, A. Afshari, L.K. Norford, Global sensitivity analysis of an urban microclimate system under uncertainty: design and case study, *Build. Environ.* 124 (2017) 153–170, <https://doi.org/10.1016/j.buildenv.2017.08.011>.
- [73] A. Salvati, P. Monti, H. Coch Roura, C. Cecere, Climatic performance of urban textures: analysis tools for a Mediterranean urban context, *Energy Build.* 185 (2019) 162–179, <https://doi.org/10.1016/j.enbuild.2018.12.024>.
- [74] I.D. Stewart, T.R. Oke, Local climate zones for urban temperature studies, *Bull. Am. Meteorol. Soc.* 93 (2012) 1879–1900, <https://doi.org/10.1175/BAMS-D-11-0019.1>.
- [75] R.E. López-Guerrero, A.S. Cruz, T. Hong, M. Carpio, Optimizing urban housing design: improving thermo-energy performance and mitigating heat emissions from buildings – a Latin American case study, *Urban Clim.* 57 (2024) 102119, <https://doi.org/10.1016/j.uclim.2024.102119>.
- [76] I.C. Fernández, T. Koplow-Villavicencio, C. Montoya-Tangarife, Urban environmental inequalities in Latin America: a scoping review, *World Dev.* Sustain. 2 (2023), <https://doi.org/10.1016/j.wds.2023.100055>.
- [77] A. Vásquez, E. Giannotti, E. Galdámez, P. Velásquez, C. Devoto, Green Infrastructure Planning to Tackle Climate Change in Latin American Cities, in: *Urban Climates in Latin America*, Springer International Publishing, Cham, 2019, pp. 329–354, [https://doi.org/10.1007/978-3-319-97013-4\\_13](https://doi.org/10.1007/978-3-319-97013-4_13).
- [78] R.G.P. da Silva, C.L. Lima, C.H. Saito, Urban green spaces and social vulnerability in Brazilian metropolitan regions: towards environmental justice, *Land Use Policy* 129 (2023), <https://doi.org/10.1016/j.landusepol.2023.106638>.
- [79] E.L.A. da Guarda, R.M.A. Domingos, S.H.M. Jorge, L.C. Durante, J.C.M. Sanches, M. Leão, I.J.A. Callejas, The influence of climate change on renewable energy systems designed to achieve zero energy buildings in the present: a case study in the Brazilian Savannah, *Sustain. Cities Soc.* 52 (2020), <https://doi.org/10.1016/j.scs.2019.101843>.
- [80] S. Liu, Y.T. Kwok, K.K.L. Lau, H.W. Tong, P.W. Chan, Development and application of future design weather data for evaluating the building thermal-energy performance in subtropical Hong Kong, *Energ. Build.* 209 (2020), <https://doi.org/10.1016/j.enbuild.2019.109696>.
- [81] A.D.C. Arul Babu, R.S. Srivastava, A.C. Rai, Impact of climate change on the heating and cooling load components of an archetypical residential room in major Indian cities, *Build Environ.* 250 (2024), <https://doi.org/10.1016/j.buildenv.2024.111181>.
- [82] G. Nunes, T. Giglio, Effects of climate change in the thermal and energy performance of low-income housing in Brazil—assessing design variable sensitivity over the 21st century, *Renew. Sustain. Energy Rev.* 168 (2022), <https://doi.org/10.1016/j.rser.2022.112885>.
- [83] M.A. Triana, R. Lamberts, P. Sassi, Should we consider climate change for Brazilian social housing? Assessment of energy efficiency adaptation measures, *Energy Build.* 158 (2018) 1379–1392, <https://doi.org/10.1016/j.enbuild.2017.11.003>.
- [84] R.E. Lopez-Guerrero, K. Verichev, J.P. Cardenas-Ramirez, M. Carpio, Urban heat islands' effects on the thermo-energy performance of buildings according to their socio-economic factors, *Dev. Built Environ.* (2024) 100566, <https://doi.org/10.1016/j.dibe.2024.100566>.
- [85] A.S. Cruz, L.E.G. Bastos, Predicting climate change and occupants' behaviour impact on thermal-energy performance of global south housing: Case study in Brazil, *Indoor Built Environ.* 33 (2024) 808–827, <https://doi.org/10.1177/1420326X231222157>.
- [86] Brazil, INI-R: Instrução Normativa Inmetro para a Classificação de Eficiência Energética de Edificações Residenciais, 2023.
- [87] L.G. Eli, A.F. Krelling, M.S. Olinger, A.P. Melo, R. Lamberts, Thermal performance of residential building with mixed-mode and passive cooling strategies: the Brazilian context, *Energ. Buildings* 244 (2021), <https://doi.org/10.1016/j.enbuild.2021.111047>.
- [88] E. Mantesi, C.J. Hopfe, K. Mourkos, J. Glass, M. Cook, Empirical and computational evidence for thermal mass assessment: the example of insulating concrete formwork, *Energ. Build.* 188–189 (2019) 314–332, <https://doi.org/10.1016/j.enbuild.2019.02.021>.
- [89] A.Q. Bhatti, Application of dynamic analysis and modelling of structural concrete insulated panels (SCIP) for energy efficient buildings in seismic prone areas, *Energ. Build.* 128 (2016) 164–177, <https://doi.org/10.1016/j.enbuild.2016.06.049>.
- [90] M. Amer, M. Hamdy, T. Wortmann, A. Mustafa, S. Attia, Methodology for design decision support of cost-optimal zero-energy lightweight construction, *Energ. Build.* 223 (2020), <https://doi.org/10.1016/j.enbuild.2020.110170>.
- [91] H.M. Cho, J.H. Park, S. Wi, S.J. Chang, G.Y. Yun, S. Kim, Energy retrofit analysis of cross-laminated timber residential buildings in Seoul, Korea: Insights from a case study of packages, *Energ. Build.* 202 (2019), <https://doi.org/10.1016/j.enbuild.2019.07.046>.
- [92] S. Lundberg, S.-I. Lee, A Unified Approach to Interpreting Model Predictions, (2017). <http://arxiv.org/abs/1705.07874>.
- [93] T. Chen, C. Guestrin, XGBoost: A scalable tree boosting system, in: *Proceedings of the ACM SIGKDD International Conference on Knowledge Discovery and Data Mining*, Association for Computing Machinery, 2016: pp. 785–794. <https://doi.org/10.1145/2939672.2939785>.
- [94] T. Hastie, J. Friedman, R. Tibshirani, *The Elements of Statistical Learning*, Springer New York, New York NY, 2001.
- [95] R. Evins, A review of computational optimisation methods applied to sustainable building design, *Renew. Sustain. Energy Rev.* 22 (2013) 230–245, <https://doi.org/10.1016/j.rser.2013.02.004>.
- [96] V. Machairas, A. Tsangrassoulis, K. Axarli, Algorithms for optimization of building design: a review, *Renew. Sustain. Energy Rev.* 31 (2014) 101–112, <https://doi.org/10.1016/j.rser.2013.11.036>.
- [97] K. Deb, A. Pratap, S. Agarwal, T. Meyarivan, *A Fast and Elitist Multiobjective Genetic Algorithm*, NSGA-II, 2002.
- [98] A.S. Cruz, E.G. da Cunha, The impact of climate change on the thermal-energy performance of the SCIP and ICF wall systems for social housing in Brazil, *Indoor Built Environ.* 31 (2022) 838–852, <https://doi.org/10.1177/1420326X211038047>.
- [99] A.S. Cruz, R.S. de Carvalho, E.G. da Cunha, Passive house alternative proposal for the Brazilian Bioclimatic Zone 8, *Int. J. Sustain. Dev. Plan.* 15 (2020) 827–833, <https://doi.org/10.18280/ijspd.150605>.
- [100] V.F. Mendes, A.S. Cruz, A.P. Gomes, J.C. Mendes, A systematic review of methods for evaluating the thermal performance of buildings through energy simulations, *Renew. Sustain. Energy Rev.* 189 (2024), <https://doi.org/10.1016/j.rser.2023.113875>.
- [101] V.F. Mendes, A.S. Cruz, A.P. Gomes, J.C. Mendes, Exploring the impact of evaluation methods on Global South building design—A case study in Brazil, *Build. Simul.* (2024), <https://doi.org/10.1007/s12273-024-1160-3>.
- [102] ISO, International Organization for Standardization 14040:2006 Environmental management – Life cycle assessment: Principles and framework, 2006.
- [103] CEN, EN 15804:2012+A2:2019 Sustainability of construction works - Environmental product declarations - Core rules for the product category of construction products, (n.d.).
- [104] ECOINVENT, Database - ecoinvent, (2025). <https://ecoinvent.org/database/> (accessed February 14, 2025).

- [105] CAIXA, SINAPI – Sistema Nacional de Pesquisa de Custos e Índices da Construção Civil, (2025). <https://www.caixa.gov.br/poder-publico/modernizacao-gestao/sinapi/Paginas/default.aspx> (accessed February 23, 2025).
- [106] INE, Instituto Nacional de Estadísticas - Edificación y construcción, (n.d.). <http://www.ine.gob.cl/estadisticas/economia/edificacion-y-construccion> (accessed February 23, 2025).
- [107] DANE, Departamento Administrativo Nacional de Estadística – Precios y Costos de Construcción, (n.d.). <https://www.dane.gov.co/index.php/estadisticas-por-tema/construccion> (accessed February 23, 2025).
- [108] INEI, Instituto Nacional de Estadística e Informática – Índice de Precios de Materiales de Construcción (IPMC), (2025). <https://www.inei.gob.pe/estadisticas/indice-de-precios-de-materiales-de-construccion-9469/> (accessed February 23, 2025).
- [109] T. Yang, M.C. Chen, C.C. Hung, Multiple attribute decision-making methods for the dynamic operator allocation problem, *Math. Comput. Simul.* 73 (2007) 285–299, <https://doi.org/10.1016/j.matcom.2006.04.002>.
- [110] C.-L. Hwang, K. Yoon, *Multiple Attribute Decision Making*, Springer Berlin Heidelberg, Berlin Heidelberg, 1981.
- [111] H.S. Shih, H.J. Shyur, E.S. Lee, An extension of TOPSIS for group decision making, *Math. Comput. Model.* 45 (2007) 801–813, <https://doi.org/10.1016/j.mcm.2006.03.023>.
- [112] E. Rodrigues, M.S. Fernandes, Overheating risk in Mediterranean residential buildings: comparison of current and future climate scenarios, *Appl. Energy* 259 (2020), <https://doi.org/10.1016/j.apenergy.2019.114110>.
- [113] E. Rodrigues, J. Parente, M.S. Fernandes, Building for tomorrow: Analyzing ideal thermal transmittances in the face of climate change in Brazil, *Appl. Energy* 355 (2024), <https://doi.org/10.1016/j.apenergy.2023.122360>.
- [114] E. Rodrigues, N.A. Fereidani, M.S. Fernandes, A.R. Gaspar, Climate change and ideal thermal transmittance of residential buildings in Iran, *J. Build. Eng.* 74 (2023), <https://doi.org/10.1016/j.jobe.2023.106919>.
- [115] Y. Yu, Y. Shao, B. Zhao, J. Yu, H. Guo, Y. Chen, Study on summer overheating of residential buildings in the severe cold region of China in view of climate change, *Buildings* 13 (2023), <https://doi.org/10.3390/buildings13010244>.
- [116] C.A. Alves, D.H.S. Duarte, F.L.T. Gonçalves, Residential buildings' thermal performance and comfort for the elderly under climate changes context in the city of São Paulo, Brazil, *Energ. Build.* 114 (2016) 62–71, <https://doi.org/10.1016/j.enbuild.2015.06.044>.
- [117] F. Rouault, F. Ossio, P. González-Levín, F. Meza, Impact of climate change on the energy needs of Houses in Chile, *Sustainability (Switzerland)* 11 (2019), <https://doi.org/10.3390/su11247068>.
- [118] F. Silvero, C. Lops, S. Montelpare, F. Rodrigues, Impact assessment of climate change on buildings in Paraguay—Overheating risk under different future climate scenarios, *Build. Simul.* 12 (2019) 943–960, <https://doi.org/10.1007/s12273-019-0532-6>.
- [119] R. Wang, S. Lu, X. Zhai, W. Feng, The energy performance and passive survivability of high thermal insulation buildings in future climate scenarios, *Build. Simul.* 15 (2022) 1209–1225, <https://doi.org/10.1007/s12273-021-0818-3>.
- [120] C. Filippín, F. Ricard, S. Flores Larsen, M. Santamouris, Retrospective analysis of the energy consumption of single-family dwellings in central Argentina. Retrofitting and adaptation to the climate change, *Renew. Energy* 101 (2017) 1226–1241, <https://doi.org/10.1016/j.renene.2016.09.064>.
- [121] C.A. Alves, F.L.T. Gonçalves, D.H.S. Duarte, The recent residential apartment buildings' thermal performance under the combined effect of the global and the local warming, *Energ. Build.* 238 (2021), <https://doi.org/10.1016/j.enbuild.2021.110828>.